



THE UNIVERSITY *of* EDINBURGH

Edinburgh Research Explorer

Erythro-myeloid progenitors contribute endothelial cells to blood vessels

Citation for published version:

Plein, A, Fantin, A, Denti, L, Pollard, J & Ruhrberg, C 2018, 'Erythro-myeloid progenitors contribute endothelial cells to blood vessels', *Nature*. <https://doi.org/10.1038/s41586-018-0552-x>

Digital Object Identifier (DOI):

[10.1038/s41586-018-0552-x](https://doi.org/10.1038/s41586-018-0552-x)

Link:

[Link to publication record in Edinburgh Research Explorer](#)

Document Version:

Peer reviewed version

Published In:

Nature

General rights

Copyright for the publications made accessible via the Edinburgh Research Explorer is retained by the author(s) and / or other copyright owners and it is a condition of accessing these publications that users recognise and abide by the legal requirements associated with these rights.

Take down policy

The University of Edinburgh has made every reasonable effort to ensure that Edinburgh Research Explorer content complies with UK legislation. If you believe that the public display of this file breaches copyright please contact openaccess@ed.ac.uk providing details, and we will remove access to the work immediately and investigate your claim.



1 **Erythro-myeloid progenitors contribute endothelial cells to blood vessels**

2
3 Alice Plein^{1,*}, Alessandro Fantin^{1,*}, Laura Denti¹, Jeffrey W. Pollard² and Christiana Ruhrberg^{1^}

4 ¹ UCL Institute of Ophthalmology, University College London, 11-43 Bath Street, London EC1V
5 9EL, UK

6 ² MRC Centre for Reproductive Health, University of Edinburgh, 47 Little France Crescent,
7 Edinburgh EH16 4TJ, UK

8
9 *contributed equally

10
11 ^Corresponding author:

12 Professor Christiana Ruhrberg, Tel.: 44 (0)20 7608 4017; email: c.ruhrberg@ucl.ac.uk

13
14 **The earliest blood vessels in the mammalian embryo are formed when endothelial cells**
15 **(ECs) differentiate from angioblasts and coalesce into tubular networks. Thereafter, the**
16 **endothelium is thought to expand solely by proliferation of pre-existing ECs. Here we show**
17 **that the earliest precursors of erythrocytes, megakaryocytes and macrophages, the yolk**
18 **sac-derived erythro-myeloid progenitors (EMPs), provide a complementary source of ECs**
19 **that are recruited into pre-existing vasculature. Whereas a first wave of yolk sac-resident**
20 **EMPs contributes ECs to the yolk sac endothelium, a second wave of EMPs colonises the**
21 **embryo and contributes ECs to intraembryonic endothelium in multiple organs, where they**
22 **persist into adulthood. By demonstrating that EMPs constitute a hitherto unrecognised and**
23 **non-redundant source of ECs, we reveal that embryonic blood vascular endothelium**
24 **expands in a dual mechanism that involves both the proliferation of pre-existing ECs and**
25 **the incorporation of ECs derived from hematopoietic precursors.**

26 Blood vessels distribute oxygen, nutrients, hormones and immune cells through the vertebrate
27 body and help remove waste molecules. Accordingly, functional blood vessel formation during
28 embryogenesis is a prerequisite for vertebrate life. Endothelial cells (ECs) form the inner lining of
29 blood vessels to contain the blood and its constituents. In addition, ECs serve as signalling hubs to
30 integrate tissue-derived and blood-borne signals to regulate vascular function. In the mammalian
31 embryo, the first ECs arise from mesenchymal precursors termed angioblasts that condense into
32 yolk sac vasculature and the paired dorsal aortae; this process is initiated on embryonic day (E)
33 7.0 in mice ¹. Subsequently, embryonic blood vascular endothelium is thought to expand in a
34 process termed angiogenesis, in which ECs proliferate within existing endothelium to increase
35 vascular diameter, extend sprouts into avascular tissue areas or remodel into smaller vessels by
36 intussusceptive growth ¹. Current consensus is therefore that embryonic ECs are a self-contained

37 cell lineage that expands by proliferation without contribution from new angioblasts or circulating
38 precursors. In contrast, circulating endothelial progenitors and their relationship to monocytes and
39 macrophages have controversially been described in adults ².

40 Monocytes and macrophages are mononuclear phagocytic cells of the innate immune system that
41 also modulate vascular growth ³. Thus, tissue-resident macrophages of the embryonic mouse
42 central nervous system (CNS), termed microglia, and macrophages in the zebrafish larval trunk
43 contact ECs at the tip of neighbouring vessel sprouts to promote their anastomosis into perfused
44 vessel loops ^{4, 5}. Microglia have similar roles in the injured adult zebrafish brain ⁶. Macrophages
45 also secrete VEGFA to stimulate vessel growth for nerve repair in adult mice ⁷. In contrast, a direct
46 contribution of macrophages or other myeloid cell (MC) types to embryonic vascular endothelium
47 has not been reported; thus, CRE recombinase expression under the control of the myeloid *Lysm*
48 or *Vav* promoters does not mark embryonic blood vascular endothelium in mice ^{8, 9}.

49 Most tissue-resident macrophages arise from erythro-myeloid progenitors (EMPs) that form in the
50 extra-embryonic yolk sac during embryogenesis and also serve as precursors for erythrocytes and
51 megakaryocytes ¹⁰⁻¹⁴. In mice, a wave of early EMPs, also referred to as primitive progenitors,
52 buds from yolk sac blood islands between E7.0 and E8.25 and by E9.0 differentiates into yolk sac
53 macrophages without monocytic intermediates ^{10, 13, 15-17}. Early yolk sac macrophages also
54 generate tissue-resident macrophages in the embryo proper, including microglia in the brain or
55 Langerhans cells and Kupffer cells in the epidermis and liver, respectively ¹⁶. A later wave of EMPs
56 buds from yolk sac endothelium from E8.25 onwards ^{10, 11, 14, 17}. These cells leave the yolk sac via
57 the circulation to colonise the liver ^{14, 18}, where they expand into monocytes that subsequently
58 colonise peripheral organs to differentiate into tissue-resident macrophages, thereby diluting the
59 pool of early EMP-derived macrophages in many organs but not the CNS ^{10, 16}.

60

61 **Lineage tracing with *Csf1r-iCre* identifies ECs in developing brain vasculature**

62 To target early EMPs ^{10, 13, 15}, microglia ^{19, 20} and other differentiated MCs ²¹, we and others have
63 used a transgene that expresses CRE recombinase under the control of the promoter for the
64 myeloid lineage gene *Csf1r* (*Fms*), which encodes the colony-stimulating factor 1 receptor CSF1R.
65 Microglia appear as amoeboid or ramified single YFP⁺ cells in hindbrains from mouse embryos
66 carrying *Csf1r-iCre* and the *Rosa^{Yfp}* CRE/*LoxP* recombination reporter, with microglia and ECs also
67 stained for isolectin B4 (IB4) (**Fig. 1a**) ¹⁹. As previously shown ⁴, the number of IB4⁺ YFP⁺ microglia
68 in the hindbrain subventricular zone increased between E10.5 and E11.5, when vessels fuse into
69 the subventricular vascular plexus (SVP), and decreased after SVP formation by E12.5, when they
70 move into deeper hindbrain layers (**Fig. 1b**). Surprisingly, *Csf1r-iCre* additionally targeted sporadic
71 elongated IB4⁺ cells that appeared bound into the endothelium and increased in number between
72 E10.5 and E12.5 alongside SVP expansion (**Fig. 1a-c; Extended Data Fig. 1a**). *Csf1r-iCre*-
73 targeting of vessel-bound cells was not an artefact caused by spontaneous recombination of the

74 *Rosa^{Yfp}* reporter or unspecific immunostaining, because *Rosa^{Yfp}* littermates lacking *Csf1r-iCre* also
75 lacked YFP staining (**Fig. 1a**). Furthermore, immunostaining of *Csf1r-iCre* hindbrains carrying
76 *CAG-Cat-Egfp* as an alternative recombination reporter or imaging of tdTomato (tdTom)
77 fluorescence in *Csf1r-iCre* hindbrains with the *Rosa^{tdTom}* reporter confirmed targeting of both
78 microglia and vessel-bound elongated cells (**Extended Data Fig. 1b,c**). The independently
79 generated *Csf1r-Mer-iCre-Mer* transgene, in which tamoxifen treatment is required for CRE
80 activation²², also targeted both vessel-bound cells and microglia in E12.5 hindbrains (**Fig. 1d**).

81 Immunolabelling of E12.5 *Csf1r-iCre;Rosa^{Yfp}* hindbrains for YFP and the macrophage marker
82 F4/80 (ADGRE1) or the pericyte marker NG2 excluded that vessel-bound YFP⁺ cells were
83 microglia/perivascular macrophages or pericytes (**Extended Data Fig. 1d,e**). Instead,
84 immunolabelling for the EC-specific transcription factor ERG and surface marker PECAM1 (CD31)
85 showed that vessel-bound, elongated *Csf1r-iCre*-targeted cells were ECs (**Fig. 1e**). Accordingly,
86 their morphology was similar to ECs targeted with CRE encoded by the *Cdh5-Cre^{ERT2}* transgene,
87 which is expressed in ECs but not microglia²³ and was activated by low dose tamoxifen treatment
88 (**Fig. 1e**). Moreover, *Csf1r-iCre*-targeted ECs formed CDH5⁺ junctions with neighbouring non-
89 targeted ECs (**Extended Data Fig. 1f**).

90 Immunolabelling of E11.5 *Csf1r-iCre;Rosa^{Yfp}* hindbrains showed that microglia were CSF1R⁺ YFP⁺,
91 as expected, but neither YFP⁻ nor YFP⁺ ECs expressed the CSF1R protein (**Extended Data Fig.**
92 **2a**). To determine whether the *Csf1r* promoter is active in ECs despite their lack of CSF1R protein
93 expression, we used a *Csf1r-Egfp* transgene that faithfully reports *Csf1r* promoter activity as EGFP
94 expression^{24, 25}. However, unlike microglia, ECs were not EGFP⁺ (**Extended Data Fig. 2b**).
95 Further, the analysis of publicly available transcriptomic datasets²⁶ showed that *Csf1r* is neither
96 expressed in E14.5 brain nor liver or lung ECs (**Extended Data Fig. 2c**). Finally, fluorescence-
97 activated cell sorting (FACS) of *Csf1r-iCre*-lineage traced (tdTom⁺) ECs and MCs with antibodies
98 for PECAM1 versus the pan-hematopoietic marker CD45 (PTPRC) showed that tdTom⁺ PECAM1⁻
99 CD45⁺ MCs expressed *Csf1r*, whereas tdTom⁺ PECAM1⁺ CD45⁻ ECs expressed *Cdh5*, but not the
100 the myeloid marker *Spi1* (*Pu.1*) or *Csf1r* (**Extended Data Fig. 2d-g**). Putative *Csf1r* expression by
101 a subset of brain ECs therefore does not explain *Csf1r-iCre*-mediated endothelial targeting.

102

103 ***Csf1r-iCre*-targeted ECs and EMPs are PU.1-independent and share spatiotemporal origins**

104 Lack of endothelial CSF1R expression suggests that *Csf1r-iCre*-targeted brain ECs arise from
105 precursors that activate *Csf1r* prior to their incorporation into hindbrain vasculature. By examining
106 *Csf1r-iCre;Rosa^{Yfp}* hindbrains from *Pu.1* (*Spi1*)-null mice, we excluded that *Csf1r-iCre*-targeted
107 ECs were derived from differentiated MCs or the recently identified tissue-resident myeloid
108 precursors of pericytes^{4,23}. Thus, we found that PU.1 deficiency prevented the formation of YFP⁺
109 F4/80⁺ IB4⁺ microglia, as expected, but did not reduce the number of YFP⁺ IB4⁺ F4/80⁻ ECs (**Fig.**
110 **1f-h**). Microglia were also absent from the striatum of *Csf1r-iCre;Rosa^{Yfp};Pu.1^{-/-}* brains on postnatal

111 day (P) 0, although YFP⁺ ECs were present (**Extended Data Fig. 2h**).

112 As PU.1 is not required for EMP formation²⁷, we investigated whether the formation of *Csf1r-iCre*-
113 targeted ECs is mechanistically linked to the emergence of *Csf1r*⁺ EMPs. E8.5 *Csf1r-Egfp* yolk
114 sacs contained clusters of round EGFP⁺ VEGFR2⁺ cells that protruded from VEGFR2⁺ endothelium
115 into the vascular lumen (**Fig. 2a**), consistent with previously described EMP budding¹⁴ and prior
116 work showing that EMPs express *Csf1r*¹⁰ and *Vegfr2*¹². *Csf1r-iCre* lineage tracing similarly
117 identified round VEGFR2⁺ cells that protruded into the yolk sac vascular lumen (**Fig. 2b**), including
118 round cells that expressed the EMP marker KIT¹⁰ and persisted in PU.1-deficient yolk sacs at E8.5
119 (**Fig. 2c; Extended Data Fig. 3a,b**). The endothelium of vessels in *Csf1r-iCre;Rosa^{Yfp}* yolk sacs
120 additionally contained larger and flatter YFP⁺ VEGFR2⁺ cells, which lacked active *Csf1r* expression
121 (compare **Fig. 2a** with **2b**). These cells also lacked KIT, but were PU.1-independent (**Fig. 2c;**
122 **Extended Data Fig. 3b**), similar to *Csf1r-iCre*-targeted hindbrain ECs.

123 Tamoxifen-induced, CRE-mediated reporter recombination is highest approximately 6 h after and
124 ends 24 h after injecting a single tamoxifen dose into a pregnant dam²⁸, allowing us to activate
125 *Csf1r-Mer-iCre-Mer;Rosa^{tdTom}* in discrete temporal windows at E8.5, E9.5 or E10.5 before
126 identifying lineage-traced cells in E12.5 yolk sacs by immunostaining (**Extended Data Fig. 3c**).
127 Yolk sac macrophages were labelled after E8.5 induction (**Extended Data Fig. 3d**), consistent with
128 their origin from early *Csf1r*⁺ EMPs¹⁰. Induction at E9.5 or E10.5 also labelled yolk sac
129 macrophages, likely because macrophages express *Csf1r* from E9.5 onwards^{13, 15}. Induction at
130 E8.5 or E9.5 additionally yielded tdTom⁺ yolk sac ECs, whereas induction at E10.5 did not
131 (**Extended Data Fig. 3d**). As EMPs are present in the yolk sac at E8.5 and E9.5, but home to the
132 liver thereafter¹⁶, their local availability makes them plausible precursors of *Csf1r-iCre*-labelled
133 yolk sac ECs. In agreement, tamoxifen induction of a *Kit^{CreERT2}* knockin allele²⁹ at E8.5, when KIT⁺
134 EMPs are in the yolk sac¹⁴, labelled VEGFR2⁺ ERG⁺ yolk sac ECs alongside macrophages
135 (**Extended Data Fig. 3e,f**).

136 A recent study showed that late wave EMPs lack *Csf1r* expression when they form¹⁰. To
137 investigate whether these EMPs express *Csf1r* after their liver homing, we paired *Csf1r-Mer-iCre-*
138 *Mer;Rosa^{tdTom}* with *Csf1r-Egfp* mice and induced pregnant dams with tamoxifen at E10.5 before
139 analysing E11.5 liver cells via FACS to distinguish differentiated MCs and EMPs^{10, 13, 14}. We
140 observed tdTom⁺ *Csf1r-Egfp*⁺ cells in the KIT⁻ CD45⁺ differentiated MC population, as expected,
141 but also in the KIT⁺ CD45^{lo} progenitor population that includes EMPs (**Fig. 3a,b; Extended Data**
142 **Fig. 3g-l**; KIT⁺ CD45⁻ cells were neither MCs nor EMPs, because they lacked CD45, tdTom and
143 EGFP). Blood cell analysis showed that cells from the *Csf1r-Egfp*⁺ tdTom⁺ KIT⁺ CD45^{lo} population
144 that includes EMPs was still circulating at E11.5 and therefore could access embryonic organ
145 vasculature (**Fig. 3a,b**).

146 To investigate whether *Csf1r* expression by late wave intraembryonic EMPs correlated with the
147 emergence of *Csf1r-iCre*-targeted hindbrain ECs, we induced *Csf1r-Mer-iCre-Mer;Rosa^{tdTom}*

148 embryos at E8.5, E9.5 or E10.5 and visualised tdTom expression in E12.5 hindbrains (**Fig. 3c**).
149 Microglia were targeted at all three stages, consistent with their origin from early *Csf1r*-expressing
150 EMPs and their active *Csf1r* expression; in contrast, hindbrain vasculature contained tdTom⁺ ECs
151 following induction at E10.5, but not E8.5 or E9.5 (**Fig. 3d**). Accordingly, intraembryonic *Csf1r*-
152 *iCre*-targeted ECs emerge at a time when late wave EMPs have moved from the yolk sac into the
153 embryo proper and have activated *Csf1r* expression¹⁰. *Kit*^{CreERT2} induction at E8.5, when both early
154 and late KIT⁺ EMPs are present in the yolk sac, caused microglia targeting (**Fig. 3e,f**), suggesting
155 that microglia can still be generated around E8.5 from KIT⁺ progenitor-derived yolk sac
156 macrophages¹¹. This approach also yielded tdTom⁺ ECs in the E12.5 hindbrain and therefore
157 corroborated that yolk sac-born EMPs can give rise to intraembryonic ECs. Lineage tracing from
158 three independent *Cre* alleles therefore suggests that EMPs can differentiate into ECs.

159

160 **The *Csf1r-iCre*-targeted EMP lineage gives rise to ECs *in vitro***

161 The myeloid and erythroid potential of EMPs has been demonstrated through *in vitro* differentiation
162 assays^{14, 30}. To investigate their endothelial potential, we FACS-isolated KIT⁻ CD45⁺ PECAM1⁻
163 differentiated MCs and the KIT⁺ CD45^{lo} PECAM1⁻ population that contains EMPs from E12.5
164 *Csf1r-iCre;Rosa^{tdTom}* liver and blood, and then used these cell populations for *in vitro* differentiation
165 that were combined with immunolabelling for myeloid and EC markers. Both populations were
166 mostly tdTom⁺ (**Fig. 4a,b**). As expected¹⁰, the EMP population was comprised of large round cells
167 with a large nucleus and little cytoplasm, whereas the MC population contained granulocytes as
168 well as monocytes in the liver and macrophages in the blood (**Fig. 4a,b**). We next cultured both
169 cell populations in methocult, which promotes the formation of hematopoietic colonies, but
170 additionally included a fibronectin substrate to facilitate EC differentiation. The differentiated
171 tdTom⁺ MCs from both the liver and blood persisted as single round/amoeboid cells (**Fig. 4c,d**) that
172 were ERG^{lo} VEGFR2^{lo} (**Fig. 4e,f**; secondary antibody only controls in **Extended Data Fig. 4a,b**). In
173 contrast, the tdTom⁺ EMP populations from both the liver and blood formed myeloid and erythroid
174 cell colonies in suspension (**Fig. 4c,d**). Moreover, both the EMP populations gave rise to single
175 adherent cells, which resembled ECs due to their spindle-shaped/elongated morphology, lacked
176 myeloid cell markers and were ERG^{hi} VEGFR2^{hi}, consistent with an EC identity (**Fig. 4e,f**;
177 **Extended Data Fig. 4b,c**). In contrast, most neighbouring, adherent round/amoeboid cells
178 expressed markers indicative of MC differentiation, including CD45, F4/80 or CSF1R (**Fig. 4e,f**;
179 **Extended Data Fig. 4c**). Together, these experiments demonstrate that EMPs have endothelial
180 potential alongside their known hematopoietic capacity.

181

182 ***Csf1r-iCre*-targeted ECs support the growth of embryonic brain vasculature**

183 *Hoxa* cluster genes regulate haematopoiesis³¹ and are upregulated in postnatal compared to adult
184 ECs³², with HOXA9 also shown to promote EC differentiation from progenitor cells in adult

185 ischemic disease³³. Our analysis of published transcriptomic data^{12, 34} revealed that several *Hoxa*
186 transcripts are enriched in E10.25 compared to E9.0 EMPs or differentiated macrophages (**Fig.**
187 **5a**). To investigate whether *Hoxa*-deficiency impaired the formation of EMP-derived ECs, we
188 crossed *Csf1r-iCre* and *Rosa^{tdTom}* into mice carrying a conditional null *Hoxa* cluster mutation
189 (*Hoxa^{fl/fl}*)³⁵ (**Extended Data Fig. 5a**). Gene copy analysis showed effective gene targeting in KIT⁺
190 cells from E12.5 *Csf1r-iCre;Hoxa^{fl/fl}* mutant compared to control livers, but the number of CD45⁺
191 cells, including differentiated MCs, was not reduced (**Extended data Fig. 5b-f**). These findings
192 suggest that *Hoxa* genes are dispensable for MC specification from late wave EMPs. In contrast,
193 significantly fewer tdTom⁺ ECs, also derived from late wave EMPs, had formed in *Csf1r-*
194 *iCre;Rosa^{tdTom};Hoxa^{fl/fl}* mutant compared to control hindbrains; moreover, SVP complexity was
195 significantly reduced in the mutant compared to control hindbrains (**Fig. 5b-d**). Although we also
196 observed 20% fewer microglia in mutant compared to control hindbrains (**Extended data Fig. 5g-**
197 **i**), this unlikely contributed to the vascular defect, because even 50% fewer microglia in *Csf1^{op/+}*
198 mutants did not reduce SVP complexity (**Extended data Fig. 5j-l**). Together, these findings
199 suggest that *Hoxa* cluster genes promote the formation of EMP-derived brain ECs, which in turn
200 support normal brain vascular development.

201

202 **The EMP-derived EC population has a core endothelial transcriptional signature with** 203 **enrichment for liver EC markers**

204 As *Csf1r-iCre*-targeted ECs appeared morphologically similar to neighbouring ECs (e.g. **Fig. 1**),
205 with similarly slow proliferation and overall cell cycle kinetics (**Extended Data Fig. 6**), we next
206 compared the gene expression signature of both EC types by RNAseq. Thus, we used E12.5
207 *Csf1r-iCre;Rosa^{tdTom}* embryos for FACS to separate tdTom⁺ and tdTom⁻ ECs, defined as PECAM1⁺
208 cells lacking KIT, CD45 and CD11b (ITGAM) (**Fig. 6a**). Both EC populations differed by their
209 expression of the *Rosa* transcript, as expected (**Extended Data Fig. 7a**), but otherwise had largely
210 similar transcriptomes with few differentially expressed genes (**Fig. 6b,c**). Consistent with an
211 endothelial identity, tdTom⁺ ECs lacked markers for differentiated MCs and other non-EC lineages,
212 but expressed transcripts for core EC markers at similar levels as tdTom⁻ ECs (**Fig. 6d,e**).
213 Amongst the differentially expressed genes, markers typical of EC specialisation were under-
214 represented in tdTom⁺ ECs, such as ephrins and their EPH receptors, which regulate
215 arteriovenous differentiation, or *Slc2a1*, a marker of brain EC maturation (**Fig. 6c,e,f**). Reverse
216 transcriptase quantitative PCR (RT-qPCR) comparisons confirmed that the brain EC maturation
217 marker *Slc2a1* was expressed at lower levels in tdTom⁺ than tdTom⁻ ECs at E12.5, consistent with
218 delayed endothelial differentiation (**Extended data Fig. 7b**). This observation agrees with the idea
219 that *Csf1r-iCre* lineage-traced ECs in the brain are derived from circulating progenitors that are
220 recruited into a vascular endothelium that is pre-formed by ECs of classical origin. Whereas *Slc2a1*
221 and other markers of brain ECs were under-represented in the embryo-wide tdTom⁺ EC

222 population, liver EC markers were over-represented (e.g. *Oit3*, *Mrc1*), including early markers of
223 liver sinusoidal differentiation (*Stab2* and *Lyve1*)³⁶ (**Fig. 6c,f**). These observations were confirmed
224 by RT-qPCR (**Extended data Fig. 7b,c**). RT-qPCR confirmed that liver transcripts were expressed
225 at similar levels in tdTom⁺ and tdTom⁻ liver ECs (**Extended Data Fig. 7d**), thereby corroborating
226 that EMP- and non-EMP-derived ECs are overall similar. Moreover, this finding suggested that the
227 over-representation of liver EC transcripts in the total embryonic EC population reflected a
228 preferential contribution of EMP-derived vascular progenitors to liver vasculature rather than
229 altered liver EC differentiation. Immunostaining and flow cytometry of *Csf1r-iCre;Rosa^{tdTom}* E12.5
230 and E18.5 embryos confirmed that tdTom⁺ ECs were more prevalent in liver endothelium than
231 tdTom⁻ ECs (**Fig. 6g,i; Extended Data Figs. 8 and 9a,b**). Agreeing with the RT-qPCR analysis,
232 MRC1 as well as LYVE1 were observed in both tdTom⁻ and tdTom⁺ ECs within E12.5 liver
233 vasculature (**Fig. 6g; Extended Data Fig. 8a**). Liver ECs of two distinct origins therefore undergo
234 similar organ-specific EC differentiation.

235

236 ***Csf1r-iCre*-targeted ECs populate multiple embryonic organs and persist into adulthood**

237 Immunostaining and FACS analyses at E18.5 confirmed that *Csf1r-iCre*-targeted ECs contribute to
238 brain and liver, but also heart and lung vasculature (**Fig. 6i; Extended Data Fig. 8 and 9a,b**).
239 EMPs therefore contribute to organ vasculature at multiple sites (working model in **Extended Data**
240 **Fig. 9c**). Corresponding immunostaining and FACS analyses of adult organs showed that tdTom⁺
241 ECs persisted in the brain, heart, lung and liver (**Fig. 6h,j; Extended Data Fig. 10**). Moreover,
242 tdTom⁺ ECs continued to dominate the LYVE1⁺ MRC1⁺ liver sinusoidal endothelium of adult mice
243 (**Fig. 6h,j; Extended Data Fig. 10b**). Accordingly, organs differ with respect to their content of
244 EMP-derived ECs, with a remarkably high contribution to liver sinusoidal endothelium in both
245 embryos and adults.

246

247 **Discussion**

248 The heterogeneous origin of blood vascular mural cells from distinct populations of mesodermal
249 progenitors, hematopoietic and neural crest cells is established³⁷. Here, we have combined
250 constitutive and temporally inducible lineage tracing with FACS, immunostaining, transcriptomic
251 analyses and cell culture assays to show that embryonic vascular endothelium has two major
252 origins: a classical origin via angioblast differentiation into ECs and the unexpected differentiation
253 of ECs from the EMP lineage. Multiple prior investigations have utilised the *Csf1r-iCre* transgene
254 together with recombination reporters to follow the embryonic myeloid lineage^{10, 13, 15}. These
255 studies predominantly employed flow cytometry with hematopoietic markers, which precluded the
256 observation of *Csf1r-iCre*-targeted ECs. In contrast, we included EC markers to isolate *Csf1r-iCre*-
257 targeted ECs alongside MCs from embryonic and adult organs. Immunostaining of tissues was

258 previously also used to identify *Csf1r-iCre*-targeted cells in the retina ²⁰, liver and colon ²¹, but
259 without description of EC targeting, possibly because of the close spatial proximity of ECs and
260 perivascular macrophages ^{4,6}. By performing high resolution imaging after immunostaining for EC
261 and macrophage makers, we have overcome this limitation to demonstrate targeting of both cell
262 types alongside each other *in situ*. The contribution of EMP-derived ECs to yolk sac, brain, heart
263 and lung vasculature is proportionally smaller than that of ECs of classical origin, whereas EMP-
264 derived ECs predominate the liver, particularly the sinusoidal endothelium. Liver endothelium was
265 previously reported to be heterogeneous in origin, with an endoderm lineage contribution of
266 approximately 15% and the remainder of the liver EC population attributed to a venous origin, i.e.
267 angiogenic ingrowth from nearby veins ³⁸. Our results suggest that liver endothelium additionally
268 contains approximately 60% EMP-derived ECs, accordingly decreasing prior estimates for liver
269 ECs of venous origin. Preferential EMP homing to the liver after their entry into the embryonic
270 circulation ¹⁶ and the dependence of liver growth on rapid vascular expansion ³⁹ may explain the
271 relatively large contribution of EMP-derived ECs to this organ. Ultimately, the discovery that EMPs
272 provide a source of ECs for organ vasculature may open up new therapeutic avenues for vessel-
273 dependent organ repair and regeneration. For example, EMPs or EMP-like EC progenitors,
274 derived from human stem cells via genetic manipulation of factors such as or including *Hoxa*
275 genes, may be delivered systemically to support vascular growth in ischemic diseases or provide
276 angiocrine signals that stimulate tissue stem cells.

277

278 **References**

- 279 1. Potente, M., Gerhardt, H. & Carmeliet, P. Basic and therapeutic aspects of angiogenesis. *Cell*
280 **146**, 873-887 (2011).
- 281 2. Hirschi, K.K., Ingram, D.A. & Yoder, M.C. Assessing identity, phenotype, and fate of
282 endothelial progenitor cells. *Arteriosclerosis, thrombosis, and vascular biology* **28**, 1584-1595
283 (2008).
- 284 3. Pollard, J.W. Trophic macrophages in development and disease. *Nature Reviews Immunology*
285 **9**, 259-270 (2009).
- 286 4. Fantin, A. *et al.* Tissue macrophages act as cellular chaperones for vascular anastomosis
287 downstream of VEGF-mediated endothelial tip cell induction. *Blood* **116**, 829-840 (2010).
- 288 5. Gerri, C. *et al.* Hif-1alpha regulates macrophage-endothelial interactions during blood vessel
289 development in zebrafish. *Nat Comm* **8**, 15492 (2017).
- 290 6. Liu, C. *et al.* Macrophages Mediate the Repair of Brain Vascular Rupture through Direct
291 Physical Adhesion and Mechanical Traction. *Immunity* **44**, 1162-1176 (2016).
- 292 7. Cattin, A.L. *et al.* Macrophage-Induced Blood Vessels Guide Schwann Cell-Mediated
293 Regeneration of Peripheral Nerves. *Cell* **162**, 1127-1139 (2015).

- 294 8. Clausen, B.E., Burkhardt, C., Reith, W., Renkawitz, R. & Forster, I. Conditional gene targeting
295 in macrophages and granulocytes using LysMcre mice. *Transgenic research* **8**, 265-277
296 (1999).
- 297 9. de Boer, J. *et al.* Transgenic mice with hematopoietic and lymphoid specific expression of Cre.
298 *European J Immunol* **33**, 314-325 (2003).
- 299 10. Hoeffel, G. *et al.* C-Myb(+) erythro-myeloid progenitor-derived fetal monocytes give rise to
300 adult tissue-resident macrophages. *Immunity* **42**, 665-678 (2015).
- 301 11. Frame, J.M., McGrath, K.E. & Palis, J. Erythro-myeloid progenitors: "definitive" hematopoiesis
302 in the conceptus prior to the emergence of hematopoietic stem cells. *Blood cells, molecules &*
303 *diseases* **51**, 220-225 (2013).
- 304 12. Mass, E. *et al.* Specification of tissue-resident macrophages during organogenesis. *Science*
305 **353** (2016).
- 306 13. Gomez Perdiguero, E. *et al.* Tissue-resident macrophages originate from yolk-sac-derived
307 erythro-myeloid progenitors. *Nature* **518**, 547-551 (2015).
- 308 14. McGrath, K.E. *et al.* Distinct Sources of Hematopoietic Progenitors Emerge before HSCs and
309 Provide Functional Blood Cells in the Mammalian Embryo. *Cell Reports* **11**, 1892-1904 (2015).
- 310 15. Schulz, C. *et al.* A lineage of myeloid cells independent of Myb and hematopoietic stem cells.
311 *Science* **336**, 86-90 (2012).
- 312 16. Ginhoux, F. & Guilliams, M. Tissue-Resident Macrophage Ontogeny and Homeostasis.
313 *Immunity* **44**, 439-449 (2016).
- 314 17. Hoeffel, G. & Ginhoux, F. Fetal monocytes and the origins of tissue-resident macrophages.
315 *Cell Immunol* (2018). doiL 10.1016/j.cellimm.2018.01.001 [Epub ahead of print]
- 316 18. Lux, C.T. *et al.* All primitive and definitive hematopoietic progenitor cells emerging before E10
317 in the mouse embryo are products of the yolk sac. *Blood* **111**, 3435-3438 (2008).
- 318 19. Fantin, A. *et al.* NRP1 acts cell autonomously in endothelium to promote tip cell function
319 during sprouting angiogenesis. *Blood* **121**, 2352-2362 (2013).
- 320 20. Stefater, J.A., 3rd *et al.* Regulation of angiogenesis by a non-canonical Wnt-Flt1 pathway in
321 myeloid cells. *Nature* **474**, 511-515 (2011).
- 322 21. Deng, L. *et al.* A novel mouse model of inflammatory bowel disease links mammalian target of
323 rapamycin-dependent hyperproliferation of colonic epithelium to inflammation-associated
324 tumorigenesis. *Am J Pathol* **176**, 952-967 (2010).
- 325 22. Qian, B.Z. *et al.* CCL2 recruits inflammatory monocytes to facilitate breast-tumour metastasis.
326 *Nature* **475**, 222-225 (2011).
- 327 23. Yamazaki, T. *et al.* Tissue Myeloid Progenitors Differentiate into Pericytes through TGF-beta
328 Signaling in Developing Skin Vasculature. *Cell Reports* **18**, 2991-3004 (2017).
- 329 24. Sasmono, R.T. *et al.* A macrophage colony-stimulating factor receptor-green fluorescent
330 protein transgene is expressed throughout the mononuclear phagocyte system of the mouse.
331 *Blood* **101**, 1155-1163 (2003).

- 332 25. Burnett, S.H. *et al.* Conditional macrophage ablation in transgenic mice expressing a Fas-
333 based suicide gene. *J Leukocyte Biol* **75**, 612-623 (2004).
- 334 26. Tam, S.J. *et al.* Death receptors DR6 and TROY regulate brain vascular development. *Dev*
335 *Cell* **22**, 403-417 (2012).
- 336 27. Kierdorf, K. *et al.* Microglia emerge from erythromyeloid precursors via Pu.1- and Irf8-
337 dependent pathways. *Nature Neuroscience* **16**, 273-280 (2013).
- 338 28. Wilson, C.H. *et al.* The kinetics of ER fusion protein activation in vivo. *Oncogene* **33**, 4877-
339 4880 (2014).
- 340 29. Klein, S. *et al.* Interstitial cells of Cajal integrate excitatory and inhibitory neurotransmission
341 with intestinal slow-wave activity. *Nat Comm* **4**, 1630 (2013).
- 342 30. Palis, J., Robertson, S., Kennedy, M., Wall, C. & Keller, G. Development of erythroid and
343 myeloid progenitors in the yolk sac and embryo proper of the mouse. *Development* **126**, 5073-
344 5084 (1999).
- 345 31. Alharbi, R.A., Pettengell, R., Pandha, H.S. & Morgan, R. The role of HOX genes in normal
346 hematopoiesis and acute leukemia. *Leukemia* **27**, 1000-1008 (2013).
- 347 32. Toshner, M. *et al.* Transcript analysis reveals a specific HOX signature associated with
348 positional identity of human endothelial cells. *PloS one* **9**, e91334 (2014).
- 349 33. Rossig, L. *et al.* Histone deacetylase activity is essential for the expression of HoxA9 and for
350 endothelial commitment of progenitor cells. *J Exp Med* **201**, 1825-1835 (2005).
- 351 34. Browning, A.C. *et al.* Comparative gene expression profiling of human umbilical vein
352 endothelial cells and ocular vascular endothelial cells. *Br J Ophthalmol* **96**, 128-132 (2012).
- 353 35. Kmita, M. *et al.* Early developmental arrest of mammalian limbs lacking HoxA/HoxD gene
354 function. *Nature* **435**, 1113-1116 (2005).
- 355 36. Nonaka, H., Tanaka, M., Suzuki, K. & Miyajima, A. Development of murine hepatic sinusoidal
356 endothelial cells characterized by the expression of hyaluronan receptors. *Dev Dyn* **236**, 2258-
357 2267 (2007).
- 358 37. Majesky, M.W. Developmental basis of vascular smooth muscle diversity. *Arteriosclerosis,*
359 *thrombosis, and vascular biology* **27**, 1248-1258 (2007).
- 360 38. Goldman, O. *et al.* Endoderm generates endothelial cells during liver development. *Stem Cell*
361 *Reports* **3**, 556-565 (2014).
- 362 39. Matsumoto, K., Yoshitomi, H., Rossant, J. & Zaret, K.S. Liver organogenesis promoted by
363 endothelial cells prior to vascular function. *Science* **294**, 559-563 (2001).
- 364

365 **Supplementary information** is available in the online version of the paper.

366

367 **Acknowledgements**

368 We thank the Biological Resources, FACS, Imaging and Genomics facilities at UCL and E. Scarpa
369 for technical help, D. Saur, A. Mass, D. Duboule, M. Kmita and Y. Kubota for mouse strains, M.

370 Golding for helpful discussions. This research was supported by grants from the Wellcome Trust
371 (095623/Z/11/Z, 101067/Z/13/Z), Medical Research Council (MR/N011511/1) and British Heart
372 Foundation (FS/17/23/32718).

373 **Author contributions**

374 A.P., A.F. and C.R. conceived and planned this study, analysed the data and co-wrote the
375 manuscript. L.D. performed genetic crosses and genotyping. A.P. and A.F. performed experiments
376 either together or replicated each other's experiments, except for the cell cycle and *Hoxa* studies,
377 which were carried out by A.P and A.F., respectively. J.W.P. provided mouse strains. C.R.
378 supervised the project. All authors reviewed and edited the manuscript.

379

380 **Author information.** Reprints and permission information is available at www.nature.com/reprints.
381 The authors declare no competing interests. Correspondence and requests for materials should be
382 addressed to C.R. (c.ruhrberg@ucl.ac.uk).

383

384 **Data availability.** All sequence data used in this study have been deposited in the NCBI Gene
385 Expression Omnibus database and are accessible through accession numbers GSExxxx.

386

387

388 **Figure legends**

389

390 **Fig. 1: *Csf1r-iCre* lineage tracing identifies ECs in developing brain vasculature.**

391 (a) Confocal z-stacks of hindbrains of the indicated genotypes and gestational stages, wholemount
392 labelled for YFP and IB4, identified *Csf1r-iCre* targeting of vessel-bound cells during hindbrain
393 vascularisation. (b) Number of YFP⁺ IB4⁺ single cells (microglia) and YFP⁺ IB4⁺ vessel-bound cells
394 (putative ECs) per 0.72 mm²; mean ± SD, n=3 hindbrains each. (c) Correlation between vessel
395 area and number of YFP⁺ putative ECs; r², coefficient of determination; P < 0.01; each data point
396 represents the value of one hindbrain.

397 (d) Confocal z-stack of an E12.5 *Csf1r-Mer-iCre-Mer;Rosa^{tdTom}* hindbrain after tamoxifen delivery
398 on E10.5, IB4 wholemount labelled and shown including tdTom fluorescence.

399 (e) Confocal z-stacks of *Csf1r-iCre;Rosa^{tdTom}* and *Cdh5-Cre^{ERT2};Rosa^{tdTom}* E12.5 hindbrains,
400 wholemount labelled for the endothelial markers ERG and PECAM1 and shown including tdTom
401 fluorescence to demonstrate that *Csf1r-iCre* targets ECs; *Cdh5-Cre^{ERT2}* was induced with a low
402 tamoxifen dose at E11.5.

403 (f-h) Confocal z-stacks of *Csf1r-iCre;Rosa^{Yfp}* E11.5 hindbrains on a *Pu.1^{+/+}* versus *Pu.1^{-/-}*

404 background, wholemount labelled for YFP and F4/80 together with IB4, show that *Csf1r-iCre*-
405 targeted ECs are PU.1-independent. The boxed area in (f) was 3D surface rendered and is shown
406 in (g) en face and as a lateral view starting at the plane indicated by the yellow line; the stippled
407 line outlines the vascular lumen (lu). (h) Quantification of YFP⁺ microglia (*Pu.1^{+/+}* n=4; *Pu.1^{-/-}* n=3)
408 and ECs (*Pu.1^{+/+}* n=6; *Pu.1^{-/-}* n=7); mean ± SD; each data point represents the value for one
409 hindbrain; n.s., non-significant, * P > 0.05 (unpaired t-test).

410 *Symbols*: Microglia and ECs are indicated with arrowheads and arrows, respectively. Solid and
411 clear symbols indicate the presence or absence of marker expression, respectively.

412 *Scale bars*: 20 μm (a,d,f), 50 μm (e).

413

414 **Fig. 2: *Csf1r-iCre*-targeted ECs emerge concomitantly with EMPs in the yolk sac.**

415 Confocal z-stacks of E8.5 yolk sacs from *Csf1r-Egfp* mice (a) or *Csf1r-iCre;Rosa^{Yfp}* mice on a
416 *Pu.1^{+/+}* versus *Pu.1^{-/-}* background (b), wholemount labelled for VEGFR2 and EGFP (a) or YFP (b).
417 Lateral views of 3D-rendered yolk sac vasculature starting at the positions indicated by cyan and
418 orange lines show lineage-traced YFP⁺ VEGFR2⁺ flat cells in the vascular wall and VEGFR2⁺
419 round cells expressing EGFP or YFP, respectively, protruding from the vascular wall into the lumen
420 (lu). *Symbols*: Wavy arrows indicate EGFP⁺ or YFP⁺ VEGFR2⁺ EMPs/MPs, straight arrows YFP⁺
421 VEGFR2⁺ ECs. *Scale bars*: 20 μm.

422

423 **Fig. 3: *Csf1r-iCre*-targeted hindbrain ECs emerge from intraembryonic EMPs.**

424 (a,b) A pregnant *Csf1r-Egfp;Csf1r-Mer-iCre-Mer;Rosa^{tdTom}* dam was injected with a single
425 tamoxifen dose on E10.5 (a) before E11.5 liver and blood cells were analysed by flow cytometry
426 (b) for CD45 and KIT, followed by gating the CD45^{hi} KIT⁻ differentiated MC (blue) and CD45^{lo} KIT⁺
427 EMP/myeloid progenitor (MP) populations (pink) for EGFP and tdTom (n=4 embryos).

428 (c-f) Pregnant *Csf1r-Mer-iCre-Mer;Rosa^{tdTom}* (c,d) and *Kit^{CreERT2};Rosa^{tdTom}* (e,f) dams were injected
429 with a single tamoxifen dose on the indicated days and confocal z-stacks obtained of E12.5
430 hindbrains after wholemount staining for the indicated markers, shown including tdTom
431 fluorescence. *Symbols*: Arrows indicate tdTom⁺ ECs, arrowheads macrophages and microglia and
432 wavy arrows a cluster of tdTom⁺ ERG⁻ IB4⁻ neural progenitors, which express *Kit* at E8.5. *Scale*
433 *bars*: 20 μm.

434

435 **Fig. 4: EMPs in the liver and blood give rise to ECs *in vitro*.**

436 (a,b) FACS gating strategy for separation of the indicated cell populations, including EMP lineage
437 cells, from E12.5 *Csf1r-iCre;Rosa^{tdTom}* liver (a) and blood (b) using antibodies for PECAM1, CD45
438 and KIT (top), including proportion of cells with tdTom recombination in the MC and EMP/MP

439 populations and Giemsa-Wright staining of representative cells (bottom); Mo, monocyte; GC,
440 granulocyte; MΦ, macrophage.

441 (c,d) Brightfield images of hematopoietic colonies formed after three days in methocult (met.); note
442 white and reddish colour of myeloid and erythroid colonies, respectively. (e,f) Fibronectin (FN)-
443 adherent cells after three days in methocult were immunolabelled for the EC markers ERG and
444 VEGFR2 and counterstained with the nuclear label DAPI. *Symbols*: Arrows indicate tdTom⁺ ECs,
445 arrowheads tdTom⁺ MCs. Solid and clear symbols indicate high versus low level expression,
446 respectively, of the indicated markers. *Scale bars*: 20 μm.

447

448 **Fig. 5: *Csf1r-iCre*-targeted ECs form in a *Hoxa*-dependent mechanism and promote**
449 **vascularisation in the embryonic hindbrain.**

450 (a) Transcriptomic analysis of the indicated cell populations, based on published RNAseq and EC
451 microarray data^{12,34} (n ≥ 2), shows that *Hoxa* genes are enriched in intraembryonic EMPs; white
452 represents low and black high relative expression levels of the indicated genes.

453 (b) Confocal z-stacks of E12.5 littermate hindbrains of the indicated genotypes, wholemount
454 labelled for F4/80, RFP to visualise tdTom and with IB4. *Symbols*: Arrows and arrowheads indicate
455 tdTom⁺ ECs and microglia, respectively. *Scale bars*: 50 μm.

456 (c) Percentage of tdTom⁺ relative to IB4⁺ EC volume in *Hoxa*^{+/+} (n=3) versus *Hoxa*^{fl/fl} mutant (n=7)
457 hindbrains on a *Csf1r-iCre;Rosa*^{tdTom} background. (d) Number of vascular branchpoints in control
458 (pooled *Csf1r-iCre*⁺;*Hoxa*^{+/+} and *Csf1r-iCre*⁻ of any *Hoxa* genotype; n=13) versus *Hoxa*^{fl/fl};*Csf1r-iCre*
459 mutant (n=9) hindbrains. Mean ± SD fold change; each data point represents the value for one
460 hindbrain; * P < 0.05 (unpaired t-test).

461

462 **Fig. 6: *Csf1r-iCre*-targeted ECs have a core endothelial transcription signature with an**
463 **increase in liver EC transcripts, and they persist in adult organ vasculature.**

464 (a) FACS of PECAM1⁺ CD45⁻ CD11b⁻ KIT⁻ cells from E12.5 *Csf1r-iCre;Rosa*^{tdTom} embryos,
465 including gating to separate tdTom⁻ and tdTom⁺ ECs for RNAseq. (b) Graphic representation of
466 genes whose expression is significantly different (green dots) or similar (black dots) between both
467 EC populations. (c) Volcano plot of 247 transcripts with on average > 100 counts that are
468 significantly different between both populations; grey and red data points represent transcripts in
469 tdTom⁻ ECs with ≥2-fold over- or under-representation, respectively, with selected genes named.
470 (d-f) Relative expression levels in both EC populations of (d) non-EC markers typical of myeloid
471 (*Cx3cr1-Ptprc*), astrocytic (*Gfap*), smooth muscle (*Acta2*), neuronal (*Rbfox3*, *Nefl*), skeletal muscle
472 (*Myog*) or epithelial (*Cdh1*) differentiation, (e) core EC or EC maturation markers and (f)
473 representative brain or liver EC specialisation markers, shown alongside their relative expression
474 in brain versus liver/lung ECs based on microarrays³¹. RNAseq analysis: mean of normalised

475 counts \pm SD, n=3 samples each (DESeq2; Benjamini-Hochberg's multiple comparisons test for p-
476 value adjustment, adjP). Microarray analysis: mean \pm SD, n=5 samples each (2-way ANOVA,
477 Bonferroni's multiple comparisons test). * P < 0.05, ** P < 0.01, *** P < 0.001, ns, non-significant.

478 **(g,h)** *Csf1r-iCre;Rosa^{tdTom}* E12.5 **(g)** and adult **(h)** liver cryosections were labelled for the indicated
479 markers and RFP to visualise tdTom, including DAPI counterstaining in **(h)**. *Symbols*: Arrows and
480 arrowheads indicate tdTom⁺ ECs and macrophages, respectively. Clear arrowheads indicate
481 VEGFR2⁻ macrophages. *Scale bar*. 50 μ m.

482 **(i,j)** The relative contribution of tdTom⁺ ECs to organ vasculature at E12.5 **(i)** and in 12-week old
483 adult mice **(j)** was determined by flow cytometry of *Csf1r-iCre;Rosa^{tdTom}* brain, heart, lung and liver.
484 Mean \pm SD; n \geq 4 (E12.5) and n \geq 6 (adult), with each data point representing an individual organ
485 (1-way ANOVA, Tukey's multiple comparisons test, ** P < 0.01, *** P < 0.001).

486

487

488 (online only) Methods plus associated references

489

490 **Mouse strains.** All animal procedures were performed in accordance with the institutional Animal
491 Welfare Ethical Review Body (AWERB) and UK Home Office guidelines. To obtain mouse
492 embryos of defined gestational age, mice were paired in the evening and the presence of a vaginal
493 plug the following morning was defined as E0.5. In some studies, we analysed adult mice, defined
494 as more than 8 weeks of age. Mice carrying the *Csf1r-iCre* transgene²¹ were mated to *Rosa^{Yfp}*⁴⁰,
495 *Rosa^{tdTom}*⁴¹ or *CAG-cat-Egfp*⁴² mice. PU.1 heterozygous null mice⁴³ were mated to *Rosa^{Yfp}* mice
496 and then *Csf1r-iCre* mice to obtain *Csf1r-iCre;Rosa^{Yfp};Pu.1^{-/-}* embryos. *Hoxa^{fl/fl}* mice³⁵ were mated
497 to *Rosa^{tdTom}* mice and then *Csf1r-iCre* to obtain *Csf1r-iCre;Rosa^{tdTom};Hoxa^{fl/fl}* embryos. *Csf1r-Mer-*
498 *iCre-Mer*²², *Cdh5-Cre-ER^{T2}*⁴⁴ and *Kit^{CreERT2}* mice²⁹ were mated to *Rosa^{tdTom}* mice. We also used
499 *Csf1r-Egfp-Ngfr/Fkbp1a/Tnfrsf6* (short: *Csf1r-Egfp*) mice as a reporter of *Csf1r* expression²⁵ and a
500 loss of function mutation in *Csf1* (*Csf1^{Op}*)⁴⁵. All mouse strains were maintained on a mixed
501 background (C57Bl6/J;129/Sv), with the exception of *Csf1r-Mer-iCre-Mer*, which was maintained
502 on a mixed FVB:C57/bl6 background. For tamoxifen induction of CRE activity, tamoxifen (Sigma)
503 was dissolved to 2 mg/ml in peanut oil and administered via intraperitoneal injection into pregnant
504 dams. For *Cdh5-Cre-ER^{T2}* and *Csf1r-Mer-iCre-Mer*, we injected 20 µg and 1 mg tamoxifen alone,
505 respectively; for *Kit^{Cre-ERT2}*, we injected 3 mg tamoxifen together with 1.75 mg progesterone
506 (Sigma).

507 **Immunolabelling.** Samples were fixed in 4% formaldehyde in PBS and processed as either
508 wholemount or 20 µm cryosections. Immunolabelling was performed as described previously⁴⁶
509 using the following antibodies and dilutions: goat anti-CDH5 (1:200; AF1002, lot FQI0116101, R&D
510 Systems), rabbit anti-CSF1R (1:500; sc-692, lot K1212, Santa Cruz), rat anti-EMCN (1:50; sc-
511 65495, lot C2917, Santa Cruz), rabbit anti-ERG (1:200; ab92513, lot GR32027 69-1, Abcam), rat
512 anti-F4/80 (1:500; MCA497R, lot 1605, Serotec), chicken anti-GFP (1:1000; GFP-1020, lot
513 0511FP12, Aves) and rabbit anti-GFP (1:500; 598, lot 079, MBL) for YFP or EGFP labelling, rabbit
514 anti-IBA1 (1:500; 019-19741, Wako Chemicals), rat anti-KIT (1:500; 553353, lot 30259, BD
515 Pharmingen), rabbit anti-NG2 (1:200; AB5320, lot 2726769, Millipore), rat anti-PECAM1 (1:200;
516 553370, lot 5205656, BD Pharmingen), rabbit anti-pHH3 (1:400; 06-570, lot 2825969, Millipore),
517 rabbit anti-RFP (1:1000; PM005, lot 045, MBL), goat anti-VEGFR2 (1:200; AF644, lot
518 COA0417021, R&D Systems). Secondary antibodies used included Alexa Fluor-conjugated goat
519 anti-chick, -rabbit or -rat IgG (Life Technologies), or, for primary antibodies raised in goat, donkey
520 fluorophore-conjugated FAB fragments of anti-chick, -goat, -rabbit or -rat IgG (Jackson
521 ImmunoResearch). Biotinylated IB4 (L2140, lot 085M4032V, Sigma) followed by Alexa-conjugated
522 streptavidin (ThermoFisher) was used to detect brain endothelial cells and microglia^{4, 19}. Nuclei
523 were labelled with DAPI. Images were acquired with a LSM710 laser scanning confocal
524 microscope (Zeiss) and processed using LSM image browser (Zeiss) and Photoshop CS4 (Adobe)
525 software. Three-dimensional rendering including surface rendering and the generation of virtual

526 slices for lateral views of high-resolution confocal z-stacks was carried out with Imaris (Bitplane).

527 **Fluorescence-activated cells sorting (FACS) and cell culture.** Tissues were mechanically and
528 enzymatically homogenised in RPMI1640 with 2.5% foetal bovine serum (ThermoFisher), 100
529 µg/ml collagenase/dispase (Roche), 50 µg/ml DNase (Qiagen) and 100 µg/ml heparin (Sigma),
530 incubated for 5 mins with 0.5 mg/ml rat Fc block (Becton Dickinson) and labelled with a
531 combination of PE/Cy7-conjugated rat anti-PECAM1 (clone 390, cat 102418, lot B212262), FITC-
532 conjugated rat anti-CD45 (clone 30-F11, cat 103108, lot B246762) or CD41 (clone MWRReg30, cat
533 133903, lot B201955), APC-conjugated rat anti-KIT (clone 2B8, cat 105812, lot B217855) and
534 PerCp/Cy5.5-conjugated rat anti-CD11b (clone M1/70, cat 101227) (all Biolegend). Appropriate
535 fluorescence gate parameters were established with unstained tissue, *Csf1r-iCre*⁻ or *Csf1r-Egfp*⁻
536 negative tissues and fluorescence-minus-one (FMO) staining. For cell cycle analysis, cell
537 populations were incubated with 10 µg/ml Hoechst 33342 (Sigma) for 30 mins at 37°C⁴⁷ before
538 labelling with PE/Cy7-conjugated rat anti-PECAM1 and performing FACS analysis. In all
539 experiments, doublets were eliminated using pulse geometry gates (FSC-H versus FSC-A and
540 SSC-H versus SSC-A), whereas dead cells were removed using SYTOX Blue (Life Technologies)
541 or LIVE/DEAD Fixable Violet (Life Technologies). Single cell suspensions were analysed using the
542 BD LSRFortessa X-20 cell analyser or sorted using the BD Influx cell sorter (BD Biosciences);
543 FlowJo software (FlowJo LLC) was used for subsequent analyses. In some experiments, a fraction
544 of each population was cytospun onto a glass slide for Wright-Giemsa staining (Sigma) followed by
545 imaging using an LSM510 microscope equipped with an AxioCam MRc camera (Zeiss). For cell
546 culture experiments, cell populations were sorted into DMEM with 100 U/ml penicillin, 100 U/ml
547 streptomycin and 20% foetal bovine serum (all ThermoFisher) before seeding the cells into a 96-
548 well plate coated with 10 µg/ml fibronectin (ThermoFisher). Cells were cultured in methocult
549 (Stemcell Technologies); haematopoietic colonies were imaged using a TS100 microscope
550 equipped with a DS-5M colour camera (Nikon). Adherent cells were fixed with 4% formaldehyde in
551 PBS and then labelled for VEGFR2, ERG, CD45, F4/80 and CSF1R (see above) before imaging
552 using a Ti-E microscope (Nikon).

553 **RNAseq.** PECAM1⁺ CD45⁻ CD11b⁻ KIT⁻ ECs were isolated from E12.5 *Csf1r-Cre;Rosa^{tdTom}*
554 embryos and divided into tdTom⁺ and tdTom⁻ populations with the Influx cell sorter before RNA
555 was extracted with the RNeasy Micro Kit (QIAGEN). cDNA was generated and amplified using the
556 SMART-seq V4 ultra low input RNA kit (Clontech). 100 pg of amplified cDNA per sample was used
557 to prepare a library with the Nextera XT kit (Illumina) and run on the NextSeq 500 sequencer
558 (Illumina). Raw sequence data were pre-processed to trim poor quality base calls and adapter
559 contamination using Trimmomatic v.0.36.4⁴⁸ and aligned to the mouse mm10 genome with STAR
560 v.2.5.2b⁴⁹. Mapped reads were deduplicated to reduce PCR bias using Picard v2.7.1.1 software
561 (<http://broadinstitute.github.io/picard/>), and the reads-per-transcript were then calculated using
562 FeatureCount v1.4.6.p5 software⁵⁰. Differential expression was performed using the BioConductor
563 package DESeq2 via the SARTools wrapper v1.3.2.0⁵¹.

564 **Reverse transcription polymerase chain reaction (PCR).** We isolated cells with the Influx cell
565 sorter (see above). We extracted RNA with the RNeasy Micro Kit and synthesised cDNA with
566 Superscript IV (ThermoFisher). Quantitative (q) RT-PCR was performed with SYBR Green on an
567 HT7900 system (Applied Biosystems) using the following oligonucleotide pairs: *Actb* 5'-
568 CACCACACCTTCTACAATGAG-3' and 5'-GTCTCAAACATGATCTGGGTC-3'; *Cdh5*
569 5'-GATGCAGATGACCCCACTGT-3' and 5'-AGGGCATCTTGTGTTCCAC-3'; *Csf1r* 5'-
570 TCGTCTACACAGTTCAGAG-3' and 5'-ATGCTGTATATGTTCTTCGGT-3'; *Spi1* 5'-
571 GCCATAGCGATCACTACTG-3' and 5'-CAAGGTTTGATAAGGGAAGC-3'; *Hoxa11* 5'-
572 TCTTTGCCTCTCTCCTTCCTT-3' and 5'-TTGCAGACGCTTCTCTTTGTT-3'; *Evx1* 5'-
573 GTGTGCTCTGGGCTCCTGT-3' and 5'-GCCAGGGTGCCTTGAGAG-3; *Slc2a1* 5'-
574 CCCAGAAGGTTATTGAGGAGT and 5'-ACAAAGAGGCCGACAGAGAA; *Mrc1* 5'-
575 ACTGGGCAATGCAAATGGAG and 5'- CCCTCAAAGTGCAATGGACA; *Oit3* 5'-
576 CGTCTGCTTCCATGTCTACTG and 5'-GTGCTCACATTCATTTTCGTCA. For each
577 oligonucleotide pair, a no-template control reaction was included.

578
579 **Microarray analysis.** Published microarray data²⁶ were used to compare gene expression levels
580 in E14.5 CD45⁻ PECAM1⁺ brain versus pooled lung and liver ECs using GEO2R software (NCBI).

581 **Statistical Analysis.** Tissues for analysis were allocated to experimental groups according to
582 genotype and gestational age. The number of YFP⁺ ECs and YFP⁺ microglia in *Csf1r-iCre;Rosa^{Yfp}*
583 hindbrains (**Fig. 1a,b** and **1f-h**) was determined in three randomly chosen 0.72 mm² regions of
584 each wholemount labelled and flatmounted hindbrain. For hindbrains in *Hoxa*-targeting
585 experiments, the number of F4/80⁺ microglia (**Extended Data Fig. 5**) and tdTom⁺ and IB4⁺ volume
586 (**Fig. 5b,c**) were determined from confocal z-stacks of four randomly chosen 0.18 mm² regions on
587 the lateral side of each hindbrain (**Extended Data Fig. 5g**). The z-stacks were surface rendered
588 with Imaris (Bitplane) to obtain the F4/80⁺, tdTom⁺ and IB4⁺ volumes, and the F4/80⁺ volume was
589 then subtracted from both the IB4⁺ and tdTom⁺ total volume to obtain the IB4⁺ EC and tdTom⁺ EC
590 volume before calculating the ratio of tdTom⁺ to IB4⁺ EC volume. To determine the number of
591 vascular intersections in *Hoxa*-targeting experiments (**Fig. 5b,d**), the same confocal z-stacks were
592 analysed with Imaris filament tracer after F4/80⁺ microglia were masked. For **Fig. 1** and **Fig. 5**, all
593 counts obtained from one hindbrain were averaged to yield the value for that hindbrain; to ensure
594 unbiased interpretation of results, the genotypes were disclosed only after data collection was
595 complete. For all experiments, we calculated the mean value for at least 3 independent samples,
596 where error bars represent the standard deviation of the mean (for details, see figure legends).
597 Comparison of medians against means justified the use of a parametric test; to determine whether
598 two datasets were significantly different, we therefore calculated p values with a two-tailed
599 unpaired Student's t test; P < 0.05 was considered significant. When more than two data sets were
600 compared, we used the statistical tests indicated in the associated figure legends. Statistical
601 analyses were performed with Excel 12.2.6 (Microsoft Office) or Prism 5 (GraphPad Software).

602 **References specific to the online methods**

- 603 40. Srinivas, S. *et al.* Cre reporter strains produced by targeted insertion of EYFP and ECFP into
604 the ROSA26 locus. *BMC Dev Biol* **1**, 4 (2001).
- 605 41. Madisen, L. *et al.* A robust and high-throughput Cre reporting and characterization system for
606 the whole mouse brain. *Nature neuroscience* **13**, 133-140 (2010).
- 607 42. Kawamoto, S. *et al.* A novel reporter mouse strain that expresses enhanced green fluorescent
608 protein upon Cre-mediated recombination. *FEBS letters* **470**, 263-268 (2000).
- 609 43. McKercher, S.R. *et al.* Targeted disruption of the PU.1 gene results in multiple hematopoietic
610 abnormalities. *The EMBO journal* **15**, 5647-5658 (1996).
- 611 44. Zarkada, G., Heinolainen, K., Makinen, T., Kubota, Y. & Alitalo, K. VEGFR3 does not sustain
612 retinal angiogenesis without VEGFR2. *Proceedings of the National Academy of Sciences of*
613 *the United States of America* **112**, 761-766 (2015).
- 614 45. Yoshida, H. *et al.* The murine mutation osteopetrosis is in the coding region of the
615 macrophage colony stimulating factor gene. *Nature* **345**, 442-444 (1990).
- 616 46. Vieira, J.M., Schwarz, Q. & Ruhrberg, C. Selective requirements for NRP1 ligands during
617 neurovascular patterning. *Development* **134**, 1833-1843 (2007).
- 618 47. Goodell, M.A., Brose, K., Paradis, G., Conner, A.S. & Mulligan, R.C. Isolation and functional
619 properties of murine hematopoietic stem cells that are replicating in vivo. *The Journal of*
620 *experimental medicine* **183**, 1797-1806 (1996).
- 621 48. Bolger, A.M., Lohse, M. & Usadel, B. Trimmomatic: a flexible trimmer for Illumina sequence
622 data. *Bioinformatics* **30**, 2114-2120 (2014).
- 623 49. Dobin, A. *et al.* STAR: ultrafast universal RNA-seq aligner. *Bioinformatics* **29**, 15-21 (2013).
- 624 50. Liao, Y., Smyth, G.K. & Shi, W. featureCounts: an efficient general purpose program for
625 assigning sequence reads to genomic features. *Bioinformatics* **30**, 923-930 (2014).
- 626 51. Varet, H., Brillet-Gueguen, L., Coppee, J.Y. & Dillies, M.A. SARTools: A DESeq2- and EdgeR-
627 Based R Pipeline for Comprehensive Differential Analysis of RNA-Seq Data. *PLoS one* **11**,
628 e0157022 (2016).

629

630 **Extended data figure legends:**

631

632 **Extended data figure 1: Endothelial *Csf1r-iCre* targeting is observed with different**
633 **recombination reporters and targeted ECs are distinguishable from macrophages and**
634 **pericytes.**

635 (a-c) Confocal z-stacks of *Csf1r-iCre;Rosa^{Yfp}* (a) *Csf1r-iCre;CAG-Cat-Egfp* (b) and *Csf1r-*
636 *iCre;Rosa^{tdTom}* (c) hindbrains at the indicated stages were wholemount labelled with IB4 and YFP
637 (a) or EGFP staining (b) or are shown together with tdTom fluorescence (c). In (a), the white
638 squares indicate areas shown in higher magnification in **Fig. 1a**. The indicated single channels are
639 also shown individually.

640 (d,e) Confocal z-stacks of E12.5 *Csf1r-iCre;Rosa^{Yfp}* hindbrains, wholemount labelled for YFP and
641 the microglia marker F4/80 (d) or the pericyte marker NG2 (e) together with IB4 show that *Csf1r-*
642 *iCre-targeted* vessel-bound cells are neither microglia nor pericytes. In (d), the boxed area is
643 shown in higher magnification and as single channels adjacent to the panel. In (e), a single optical
644 y/z cross section at the position indicated with the yellow line is displayed at higher magnification
645 with single channels.

646 (f) Confocal z-stacks of a *Csf1r-iCre;Rosa^{tdTom}* E12.5 hindbrains, wholemount labelled for ERG and
647 CDH5 and shown including tdTom fluorescence to demonstrate that *Csf1r-iCre* targets *bona fide*
648 ECs that form junctions with neighbouring ECs.

649 *Symbols:* Microglia and ECs are indicated with arrowheads and arrows, respectively, pericytes with
650 double arrowheads, junctional CDH5 staining with a curved arrow. Solid and clear symbols
651 indicate the presence or absence of marker expression, respectively. *Scale bars:* 100 μm (a), 20
652 μm (b-e), 50 μm (f).

653

654 **Extended data figure 2: Endothelial *Csf1r-iCre*-targeting is not caused by endothelial *Csf1r***
655 **expression and occurs independently of myeloid differentiation.**

656 (a,b) Confocal z-stacks of E11.5 *Csf1r-iCre;Rosa^{Yfp}* (a) or *Csf1r-Egfp* (b) hindbrains, wholemount
657 labelled for CSF1R and YFP or EGFP together with IB4, show lack of CSF1R protein and promoter
658 activity in embryonic ECs.

659 (c) Graphic representation of relative *Cdh5* and *Csf1r* expression levels in E14.5 brain or pooled
660 lung/liver EC microarrays³¹; n = 5 each; *** P > 0.001 (unpaired t-test).

661 (d-f) FACS separation of tdTom⁺ cells from *Csf1r-iCre;Rosa^{tdTom}* embryos, including (d)
662 representative gating strategy to exclude dead cells and doublets in this and subsequent
663 experiments and (e) sorting into PECAM1⁺ CD45⁻ ECs versus CD45⁺ PECAM1⁻ MCs for RT-qPCR
664 analysis. (f) Representative gene amplification graphs for *Csf1r* versus *Actb* from tdTom⁺ MCs and

665 ECs; ΔR_n , normalised reporter value for SYBR Green minus baseline instrument signals. (g)
666 Graphic representation of the fold change in amplification of the indicated genes relative to *Actb* for
667 both cell populations. Each data point represents the value of one embryo; n=3 each; * P > 0.05,
668 *** P > 0.001 (unpaired t-test).

669 (h) Confocal z-stacks of *Csf1r-iCre;Rosa^{Yfp}* P0 striatum on a *Pu.1^{+/+}* versus *Pu.1^{-/-}* background,
670 wholemount labelled for YFP and F4/80 together with IB4, show that *Csf1r-iCre*-targeted ECs are
671 PU.1-independent.

672 *Symbols*: Arrowheads indicate microglia, arrows YFP⁺ ECs, clear arrows YFP⁺ ECs that are
673 CSF1R⁻ and F4/80⁻.

674 *Scale bars*: 20 μ m.

675

676 **Extended data figure 3: Lineage tracing of yolk sac and liver EMPs.**

677 (a,b) Confocal z-stacks of wholemount labelled E8.5 wild type (a) and *Pu.1^{-/-}* (b) yolk sacs on a
678 *Csf1r-iCre;Rosa^{Yfp}* background, labelled for YFP and KIT, show *Csf1r-iCre*-targeted KIT⁺ round
679 cells corresponding to EMPs/MPs and *Csf1r-iCre*-targeted KIT⁻ flat cells corresponding to ECs.

680 (c-f) Pregnant *Csf1r-Mer-iCre-Mer;Rosa^{tdTom}* (c,d) and *Kit^{CreERT2};Rosa^{tdTom}* (e,f) dams were injected
681 with a single tamoxifen dose on the indicated days; confocal z-stacks of E12.5 yolk sacs,
682 immunolabelled for the indicated markers, show *Csf1r-iCre*-targeted ECs and macrophages.

683 *Symbols*: Wavy arrows indicate EMPs, straight arrows *Csf1r-iCre*-lineage traced ECs, arrowheads
684 macrophages. Solid and clear symbols indicate the presence or absence, respectively, of the
685 indicated markers. *Scale bars*: 20 μ m.

686 (g-i) Pregnant dams were injected with a single tamoxifen dose on E10.5 (g) before analysis of
687 E11.5 liver cells from *Csf1r-Egfp;Csf1r-Mer-iCre-Mer;Rosa^{tdTom}* (h; n=4 embryos) or *Csf1r-Mer-*
688 *iCre-Mer;Rosa^{tdTom}* embryos lacking *Csf1r-Egfp* (i; n=4 embryos) by flow cytometry for CD45 and
689 KIT; the CD45^{hi} KIT⁻ differentiated MC (blue), CD45^{lo} KIT⁺ EMP/myeloid progenitor (MP) (pink)
690 and CD45⁻ KIT⁺ populations (grey) were gated further for *Csf1r-Egfp* and tdTom.

691

692 **Extended data figure 4: Immunostaining controls for the analysis of cultured *Csf1r-iCre*-** 693 **targeted cells.**

694 The indicated cell populations were isolated by FACS from E12.5 *Csf1r-iCre;Rosa^{tdTom}* livers or
695 blood and cultured for three days in methocult before adherent cells were stained. In the first panel
696 in each row, the phase contrast and DAPI images were merged. In panels 2-4 in each row,
697 immunolabelled cells are visualised together with tdTom fluorescence, with single channels for the
698 indicated markers shown separately in grey scale. In (a,b), adherent cells from tdTom⁺ liver MC (a)

699 and EMP/MP (b) cultures were stained for ERG and VEGFR2 (top panels) or with secondary
700 antibodies only (bottom panels). In (c), adherent cells from tdTom⁺ blood EMP/MP cultures were
701 immunostained for CSF1R together with the myeloid markers CD45 (top panels) or F4/80 (bottom
702 panels). Symbols: Arrows indicate tdTom⁺ ECs, arrowheads tdTom⁺ myeloid cells. Solid and clear
703 symbols indicate the presence or absence, respectively, of the indicated markers. Abbreviations:
704 met, methocult; FN, fibronectin. Scale bars: 20 μm.

705

706 **Extended data figure 5: *Csf1r-iCre*-mediated *Hoxa* ablation impairs the EMP lineage.**

707 (a-f) Schematic representation of the *Hoxa* cluster and adjacent *Evx1* gene, including position of
708 the *LoxP* sites used for gene targeting. (b) FACS strategy to isolate KIT⁺ cells from control (pooled
709 *Csf1r-iCre*⁻ or *Csf1r-iCre*⁺;*Hoxa*^{+/+}; n=14), *Hoxa*^{+/fl};*Csf1r-iCre* heterozygous (n=6) and E12.5
710 *Hoxa*^{fl/fl};*Csf1r-iCre* mutant livers (n = 8). (c) qPCR analysis of *Hoxa* gene copy number relative to
711 *Evx1*. Data are shown as mean ± SD; each symbol represents the value for one individual liver; * P
712 < 0.05, *** P < 0.001 (1-way ANOVA, Tukey's multiple comparisons test). (d-f) Representative
713 FACS analysis (d) and quantification (e,f) of liver cell populations at E12.5 shows a similar number
714 of CD45⁺ or CD45⁺ CD11b⁺ cells (differentiated MCs) in control (pooled *Csf1r-iCre*⁻ or *Csf1r-*
715 *iCre*⁺;*Hoxa*^{+/+}, n=25 for CD45⁺ and n=17 for CD45⁺ CD11b⁺) versus *Hoxa*^{fl/fl};*Csf1r-iCre* (n=7 for
716 CD45⁺ and n=6 for CD45⁺ CD11b⁺). Mean ± SD fold change in mutants compared to control; each
717 data point represents the value for one hindbrain; ** P < 0.01; ns, non-significant (unpaired t-test).

718 (g-i) E12.5 hindbrains of the indicated genotypes were immunolabelled to determine vascular
719 complexity and microglia. (g) Schematic representation of embryonic hindbrain position (left) and
720 location of the hindbrain areas i-iv used for quantification in each hindbrain (right); values for the
721 four areas in each hindbrain were averaged to obtain the value for that hindbrain; EC
722 quantifications are shown in Fig. 5c. (h) Confocal z-stacks after wholemount labelling with IB4 and
723 for RFP to visualise tdTom and F4/80 to visualise microglia; the white boxes indicate areas shown
724 in higher magnification in Fig. 5. (i) Quantification of microglia number in *Hoxa*^{fl/fl};*Csf1r-iCre*
725 mutants (n=9) versus controls (n=10, pooled *Csf1r-iCre*⁺;*Hoxa*^{+/+} and *Csf1r-iCre*⁻ of any *Hoxa*
726 genotype). Mean ± SD fold change in mutant compared to control hindbrain; each data point
727 represents the value for one hindbrain; ** P < 0.01 (unpaired t-test).

728 (j-l) Confocal z-stacks of E11.5 *Csf1*^{+/+} and *Csf1*^{+/op} littermate hindbrains, wholemount labelled for
729 F4/80 together with IB4 (j) before quantification of the number of microglia (k) and vascular
730 branchpoints (l); note that a 50% microglia reduction in *Csf1*^{+/op} compared to *Csf1*^{+/+} hindbrains did
731 not reduce vascular complexity. Mean ± SD; each data point represents the value for one
732 hindbrain, n=3 each; ** P < 0.01; ns, non-significant (unpaired t-test).

733 Scale bars: 200 μm (h), 100 μm (j).

734

735 **Extended data figure 6: *Csf1r-iCre*-targeted ECs proliferate in vivo.**

736 **(a,b)** Confocal z-stacks of E12.5 *Csf1r-iCre;Rosa^{tdTom}* wholemount yolk sac **(a)** or hindbrain **(b)**
737 after staining for the proliferation marker pHH3 and VEGFR2 or for pHH3 together with IB4,
738 respectively, and shown together with tdTom fluorescence. The areas indicated with white squares
739 are shown in higher magnification below the corresponding panel, with tdTom and pHH3 channels
740 also shown separately in grey scale. *Symbols:* The arrows indicate proliferating tdTom⁺ pHH3⁺
741 ECs. Solid and clear symbols indicate the presence or absence, respectively, of tdTom
742 fluorescence. The wavy arrow indicates a tdTom⁻ pHH3⁺ neural progenitor. *Scale bars:* 200 μm
743 (top panels), 20 μm (lower panels).

744 **(c-e)** *Cell cycle distribution of tdTom⁺ and tdTom⁻ ECs.* **(c)** FACS gating strategy to isolate tdTom⁺
745 and tdTom⁻ PECAM1⁺ cells from E12.5 *Csf1r-iCre;Rosa^{tdTom}* embryos. **(d)** Graphic representation
746 of cell distribution based on Hoechst 33342 fluorescence as a measure of DNA content; low and
747 high staining intensity is observed in cells with a DNA ploidy of 2n, i.e. G0/G1 phase, or 4n, i.e.
748 G2/M phase, respectively; an intermediate staining intensity corresponds to S phase. **(e)**
749 Quantification of the proportion of tdTom⁺ and tdTom⁻ PECAM1⁺ cells in the G1, S and G2/M
750 phases based on the area of the corresponding peaks in **(d)**. Mean ± SD, n = 3 each; n.s., non-
751 significant (paired t-test).

752

753 **Extended data figure 7: Validation of gene expression data from RNAseq and microarray**
754 **studies.**

755 ECs were isolated by FACS as in **Fig. 6a** for validation of RNAseq and microarray data presented
756 in **Fig. 6d-f**.

757 **(a)** Relative transcript levels of the *Rosa26* locus by RNAseq of E12.5 tdTom⁺ and tdTom⁻ EC
758 populations, whose analysis is presented in **Fig. 6a-f**; mean ± SD of normalised counts, n=3 each;
759 ** P < 0.01 (unpaired t-test).

760 **(b)** RT-qPCR analysis for the indicated genes in tdTom⁺ versus tdTom⁻ ECs isolated from the
761 whole embryo (n=5) to validate differentially expressed genes identified via RNAseq in **Fig. 6e,f**.

762 **(c)** RT-qPCR analysis for the indicated genes in tdTom⁻ ECs isolated from the brain and liver (n=3
763 each) to validate organ-specific transcript enrichment identified via microarray analysis in **Fig. 6f**.

764 **(d)** RT-qPCR analysis for the indicated genes to directly compare the expression levels of brain
765 and liver EC differentiation markers in tdTom⁺ versus tdTom⁻ ECs isolated from brain (n=3) or liver
766 (n=5) **(d)** at E12.5.

767 *Slc2a1* was analysed as a representative brain EC-enriched transcript/differentiation marker, *Mrc1*
768 and *Oit3* as representative liver EC-enriched transcripts. Mean ± SD of fold change; * P < 0.05, **
769 P < 0.01, *** P < 0.001; ns, non-significant (unpaired t-test); ND, not detectable.

770 **Extended data figure 8: *Csf1r-iCre*-targeted ECs contribute to embryonic organ vasculature.**

771 (a) Cryosections of the indicated organs from E12.5 *Csf1r-iCre;Rosa^{tdTom}* mice were
772 immunolabelled for the indicated EC markers together with antibodies for RFP to identify tdTom
773 protein (top and bottom panels) or are shown with tdTom fluorescence (middle panels); single
774 channels are shown in grey scale. The white boxes indicate the position of areas shown in higher
775 magnification in **Fig. 6g**; note that some areas selected for higher magnification are not contained
776 entirely within the field of view, and accordingly the boxes are not complete. *Scale bars*: 200 μ m.

777 (b) Gating strategy for flow cytometry of dissociated cells from E12.5 *Csf1r-iCre;Rosa^{tdTom}* embryos
778 and a control sample lacking *iCre* after staining with antibodies for CD11b, CD41, CD45, KIT,
779 PECAM1 to determine the relative contribution of tdTom⁺ versus tdTom⁻ ECs to vasculature in the
780 brain, lung, heart and liver (associated quantifications shown in **Fig. 6i**; an analogous strategy was
781 used for the quantifications shown in **Fig. 6j** and in the **Extended Data Fig. 9b**).

782

783 **Extended data figure 9: *Csf1r-iCre*-targeted ECs contribute to organ vasculature in late**
784 **stage embryos.**

785 (a) Cryosections of the indicated organs from E18.5 *Csf1r-iCre;Rosa^{Yfp}* mice were immunolabelled
786 for YFP, PECAM1 and the macrophage marker IBA1; single channels are shown in grey scale.
787 *Symbols*: Arrowheads indicate YFP⁺ and IBA1⁺ macrophages; solid and empty arrows indicate ECs
788 that are YFP⁺ and lack IBA1 expression, respectively. *Scale bars*: 20 μ m.

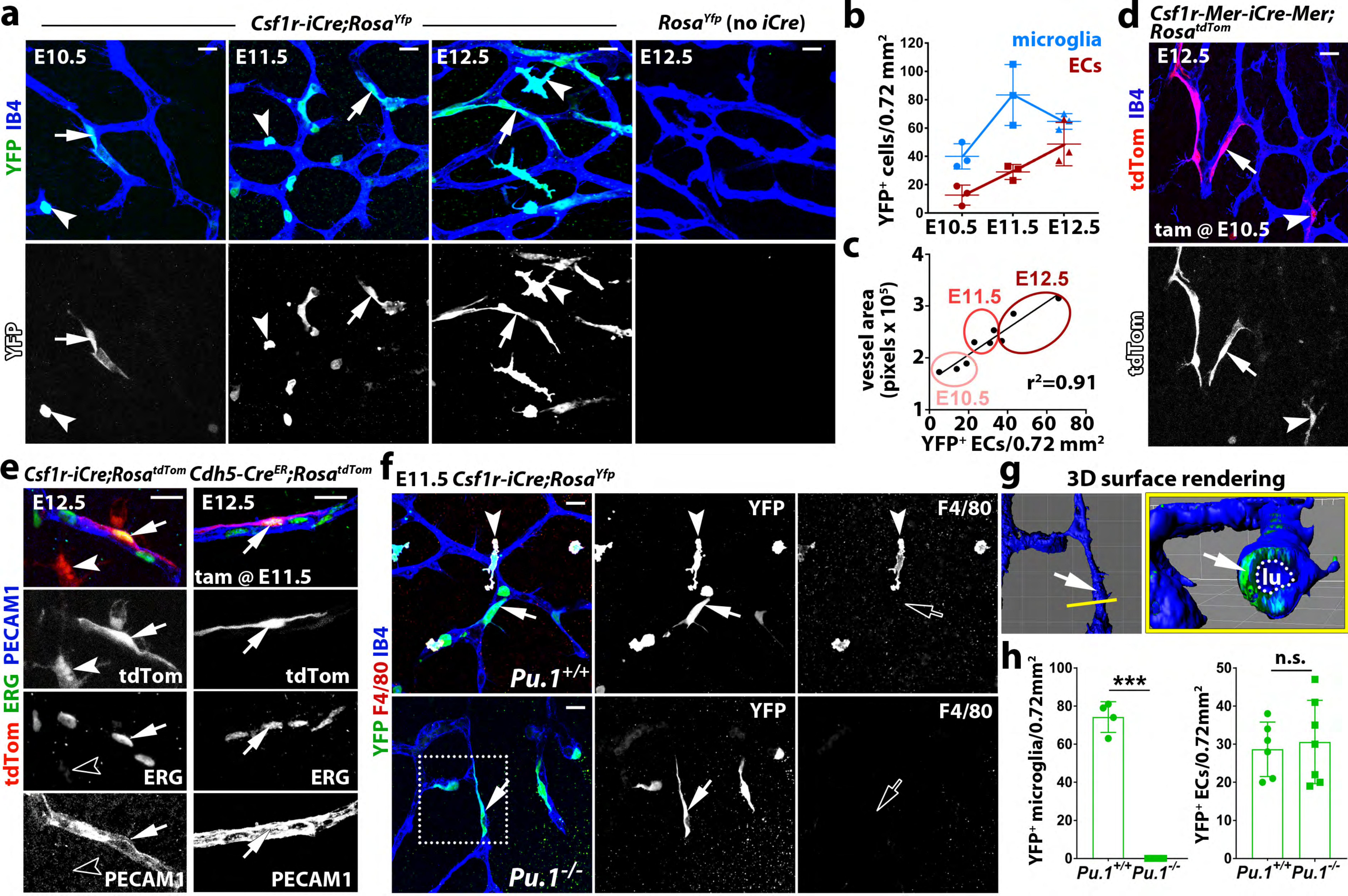
789 (b) Flow cytometry of dissociated cells from the indicated organs of E18.5 *Csf1r-iCre;Rosa^{tdTom}*
790 embryos after staining with antibodies for CD11b, CD41, CD45, KIT, PECAM1, using the gating
791 strategy shown in the **Extended data Fig. 8a**; mean \pm SD, n = 5 each; *** P > 0.001 (1-way
792 ANOVA, Tukey's multiple comparisons test).

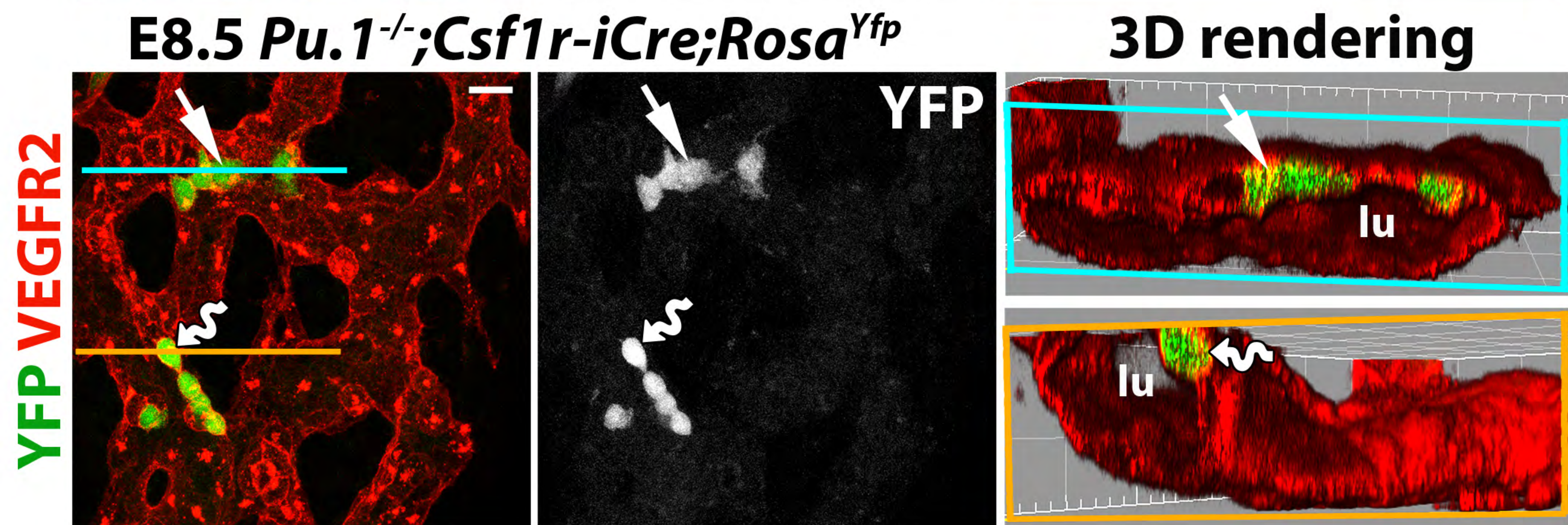
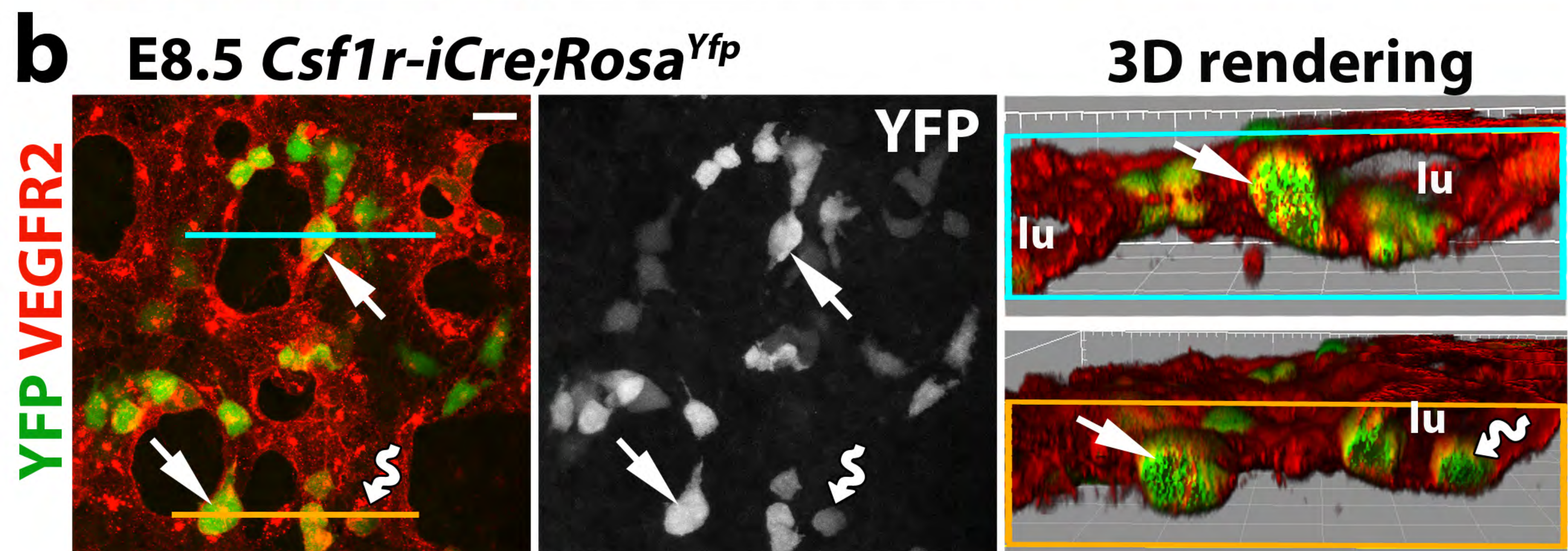
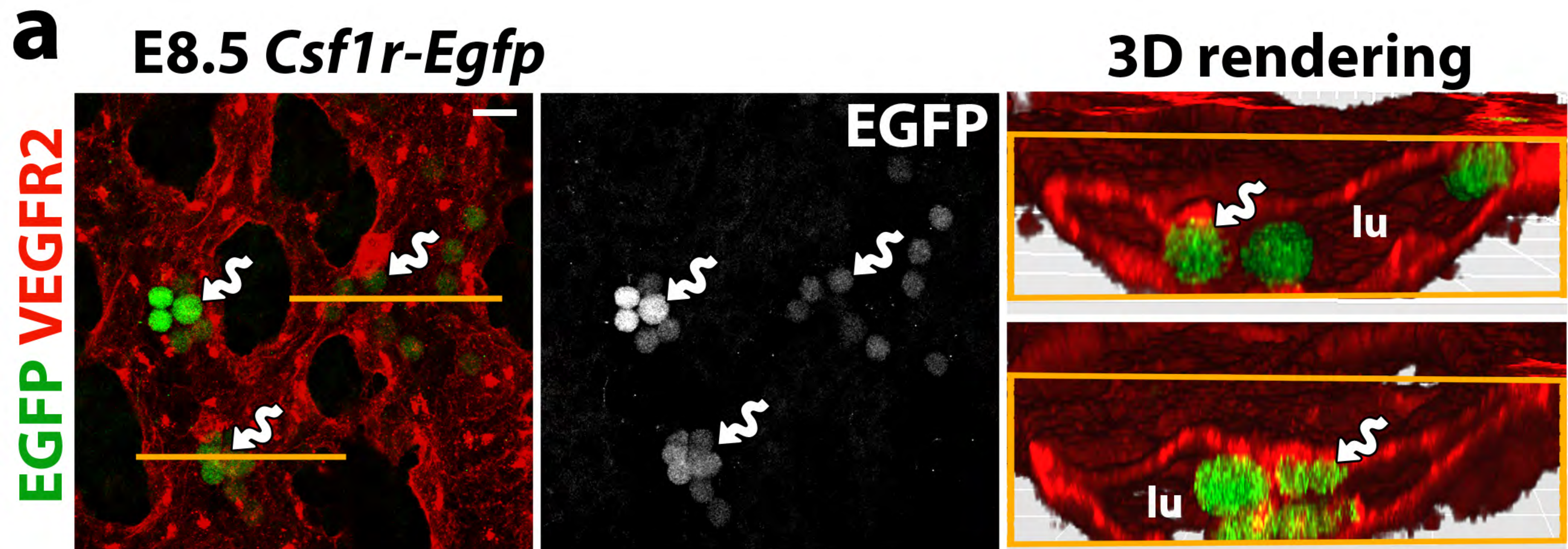
793 (c) Working model for the role of EMPs in generating extra-embryonic yolk sac and intra-
794 embryonic organ ECs alongside their known role in generating myeloid and
795 erythrocyte/megakaryocyte cells.

796

797 **Extended data figure 10: *Csf1r-iCre*-targeted ECs contribute to adult organ vasculature.**

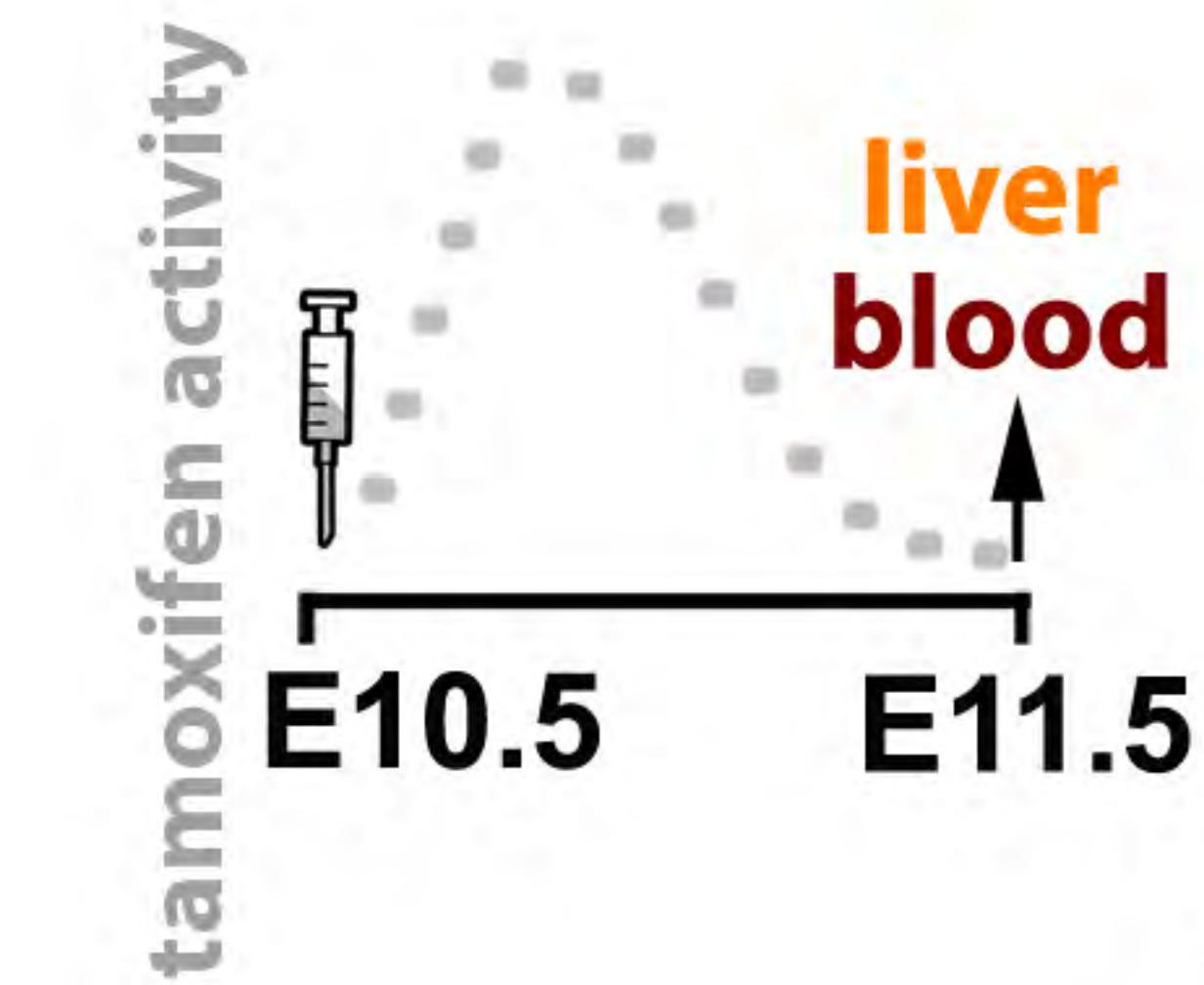
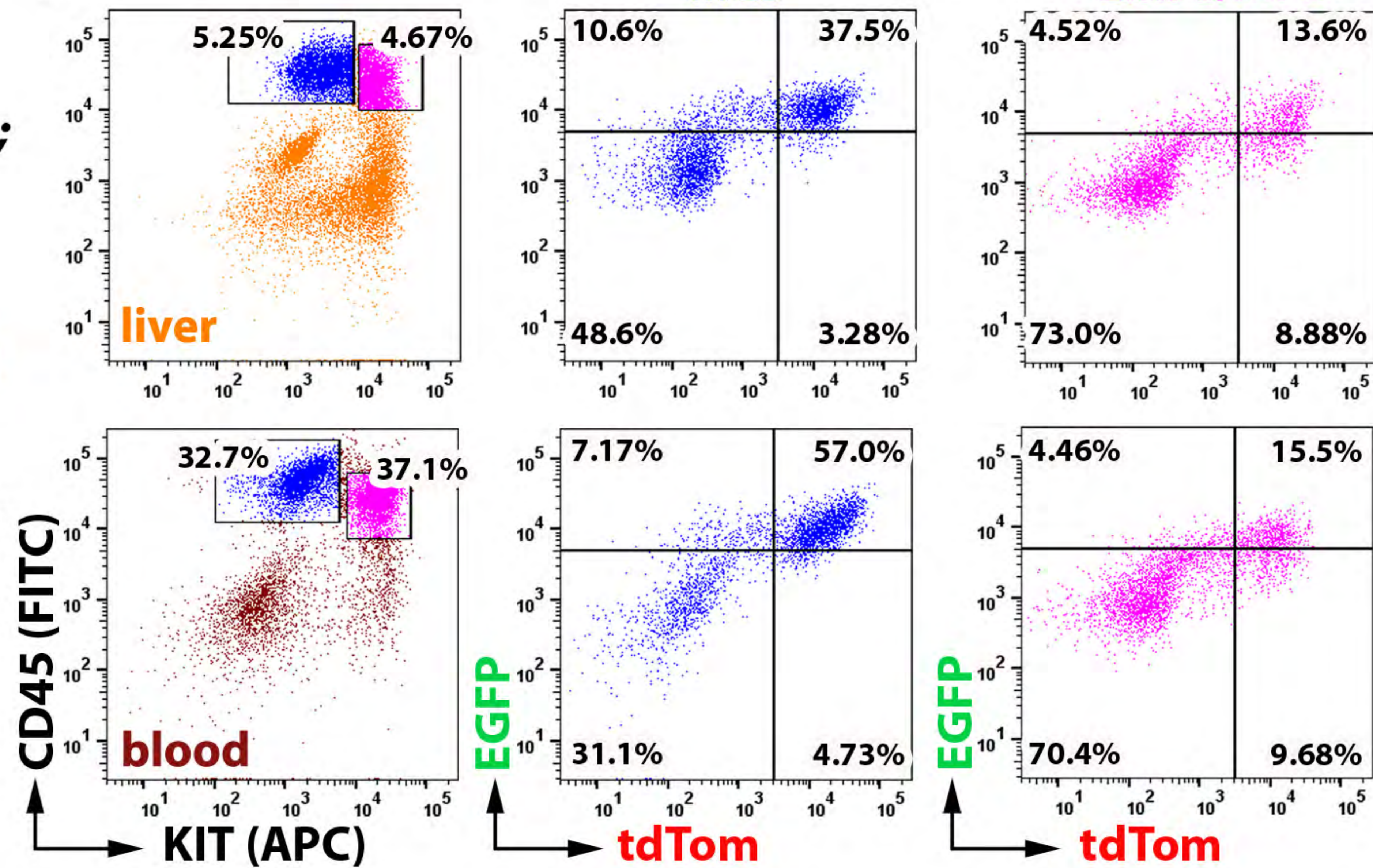
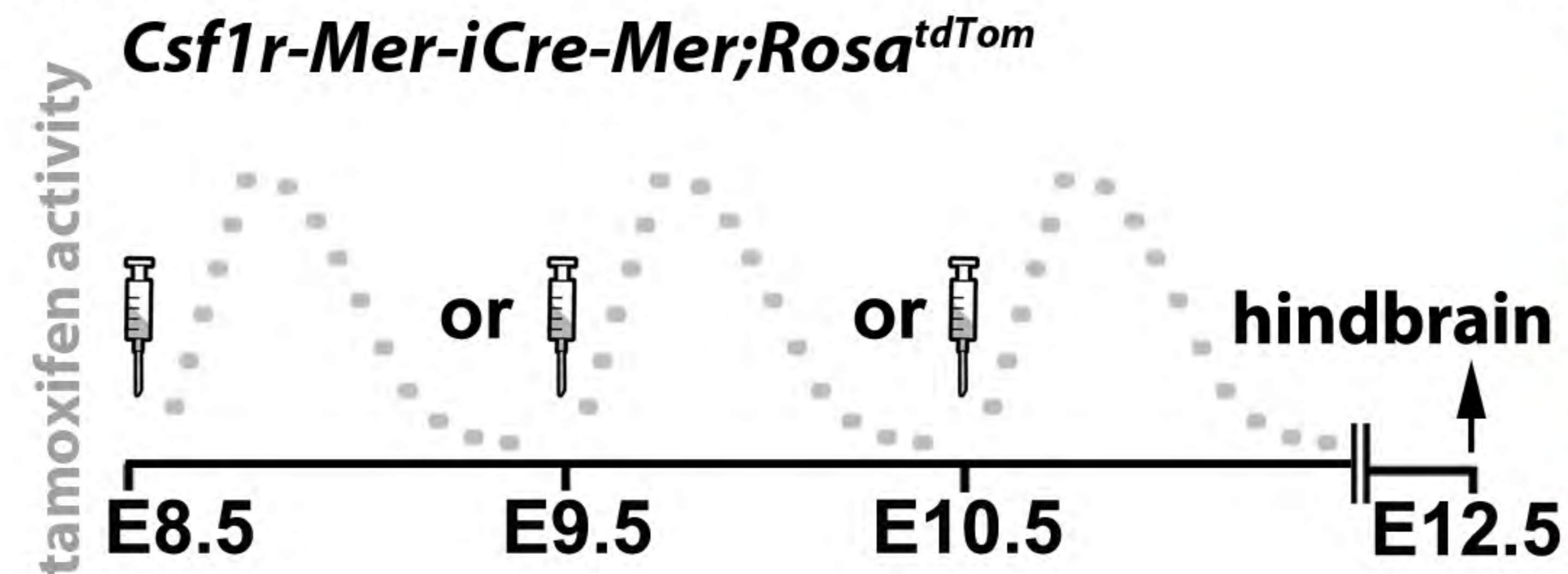
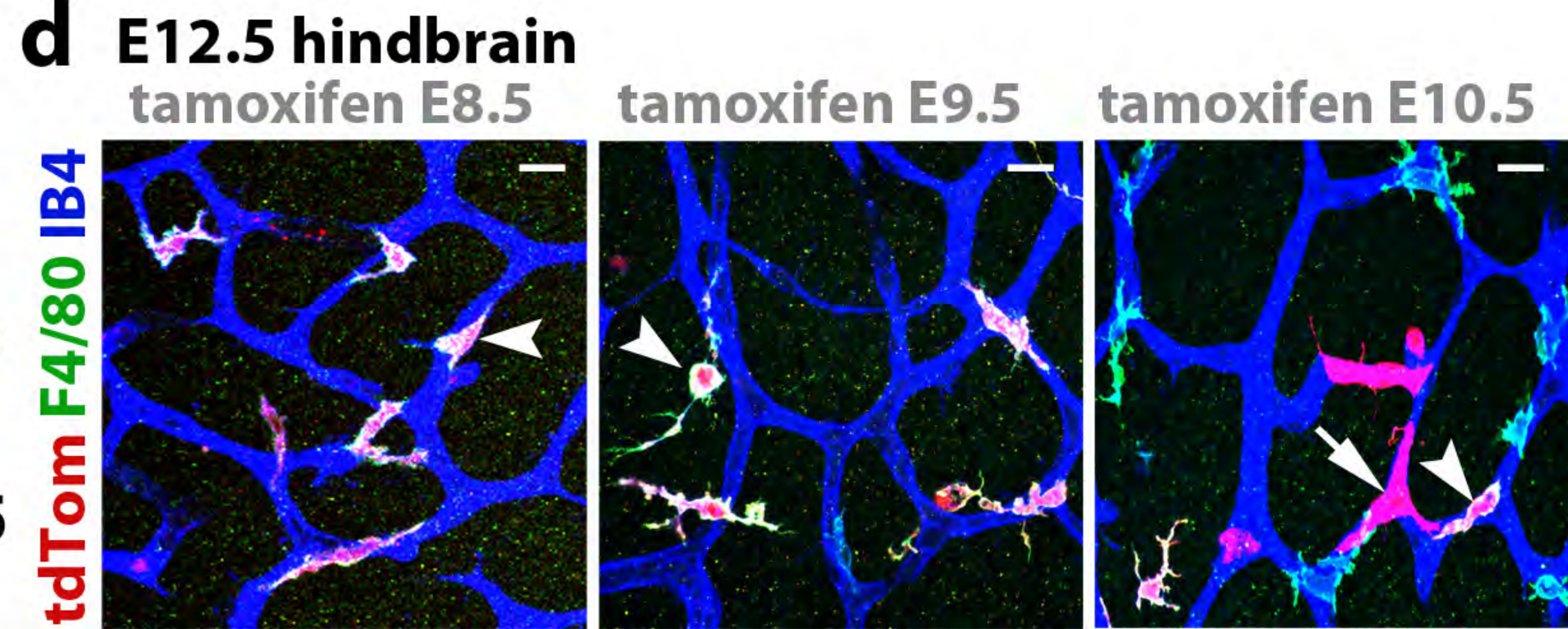
798 Cryosections of the indicated organs from 6 months old adult *Csf1r-iCre;Rosa^{Yfp}* (a) or 3 months
799 old adult *Csf1r-iCre;Rosa^{tdTom}* (b) mice were immunolabelled for the indicated EC and macrophage
800 markers together with antibodies for YFP or RFP; single channels are shown in grey scale. The
801 white box in (b) indicates an area shown in higher magnification in **Fig. 6h**. *Symbols*: Arrowheads
802 indicate YFP⁺ and F4/80⁺ macrophages; solid and empty arrows indicate ECs that are YFP⁺ and
803 lack F4/80 expression, respectively. *Scale bars*: 20 μ m (a), 100 μ m (b).





a

Csf1r-Egfp;
Csf1r-Mer-iCre-Mer;
Rosa^{tdTom}

**b****c****d****e****f**